AMES

NASA Technical Memorandum 88252

Methods for Assessing Wall Interference in the 2- by 2-Foot Adaptive-Wall Wind Tunnel

Edward T. Schairer

June 1986

National Aeronautics and Space Administration

NASA Technical Memorandum 88252

Methods for Assessing Wall Interference in the 2- by 2-Foot Adaptive-Wall Wind Tunnel

Edward T. Schairer, Ames Research Center, Moffett Field, California

June 1986

National Aeronautics and
Space Administration

Ames Research Center
Moffett Field, California 94035

SUMMARY

This paper discusses two types of methods for assessing two-dimensional wall interference in the adaptive-wall test section of the NASA Ames 2- by 2-Foot Transonic Wind Tunnel: (1) methods for predicting free-air conditions near the walls of the test section ("adaptive-wall" methods) and (2) methods for estimating wall-induced velocities near the model ("correction" methods). All of these methods are based on measurements of either one or two components of flow velocity near the walls of the test section. Each method is demonstrated using simulated wind tunnel data and is compared with other methods of the same type. The two-component adaptive-wall and correction methods were found to be preferable to the corresponding one-component methods because (1) they are more sensitive to, and give a more complete description of, wall interference; (2) they require measurements at fewer locations; (3) they can be used to establish free-stream conditions; and (4) they are independent of a description of the model and constants of integration.

INTRODUCTION

Since the early 1970s, wind tunnel engineers have recognized that flow measurements at or near the walls of a test section can be used to estimate wall interference. Such measurements were first used in adaptive-wall test sections to determine wall settings for zero interference. Subsequently the same measurements have been used in conventional as well as adaptive test sections to correct aerodynamic data for wall interference.

A variety of measured-flow boundary-condition methods is now available for assessing wall interference in wind tunnels. These methods differ in the types of flow measurements required, locations where the measurements must be made, and simplifying assumptions upon which each method is based.

In this paper, several measured-flow boundary-condition methods are described and compared to determine which are best suited for use in the new adaptive-wall test section being built for the NASA Ames 2- by 2-Foot Transonic Wind Tunnel. As this test section is designed for testing two-dimensional airfoils, only two-dimensional methods will be discussed. The paper will begin with a brief description of the 2- by 2-ft adaptive-wall test section. Following will be discussions of (1) methods for computing free-air conditions near the walls of adaptive-wall wind tunnels ("adaptive-wall" methods) and (2) methods for estimating wall-induced flow near the model ("correction" methods). A subsequent section will describe how these

methods were implemented for the present study. Finally, the adaptive-wall and correction methods will be demonstrated using simulated wind tunnel data. Derivations of the methods are not included, but are available in the references cited.

SYMBOLS

A	model cross-sectional area/c
c	model chord
C	constant of integration
C_ℓ	lift coefficient
h	tunnel height
M	Mach number
n	normal component
u	streamwise perturbation velocity
U	free-stream velocity
w	vertical velocity
x,ξ	distance downstream from model leading edge
y,η	distance above model
α	angle of attack, deg
β	$\sqrt{1 - M_\infty^2}$
q	ratio of specific heats (= 1.4 in air)
ϕ	perturbation velocity potential

Subscripts

d	most downstream point where velocity is measured
f	free-air
ff	far-field

i wall-induced

s caused by elementary singularities

u most upstream point where velocity is measured

1 inner contour

2 outer contour

∞ free-stream

Superscripts

$-$ symmetric component, $\bar{a}(x,y) = \frac{a(x,y) + a(x,-y)}{2}$

$\sim$ antisymmetric component, $\tilde{a}(x,y) = \frac{a(x,y) - a(x,-y)}{2}$

TWO- BY TWO-FOOT ADAPTIVE-WALL TEST SECTION

The 2- by 2-ft adaptive-wall test section (fig. 1) is designed to test two-dimensional airfoils at Mach numbers up to 1.0. The upper and lower walls will be slotted and the side walls will be solid. Wall interference will be minimized by regulating the airflow through the upper and lower walls.

Spanwise partitions will divide separate plenums above and below the test section into 32 compartments each. The pressure in each compartment, and thus the local airflow through the wall, will be controlled by the position of a valve connecting each compartment to two reservoirs of air, one at a higher pressure and the other at a lower pressure than that of the test section.

Each sidewall will contain a Schlieren-quality glass window extending nearly the entire height and length of the test section. The model will be supported at its aerodynamic center by self-aligning bearings mounted in the glass. The view through the windows will be unobstructed except for these bearings, a narrow support arm which will resist the model pitching moment, and a 3-in.-wide window frame.

A fast-scanning laser velocimeter, mounted between upstream and downstream bulkheads, will be capable of measuring two components of flow velocity at nearly any point in the plane midway between the sidewalls. With this unique flow-measurement capability, this test section will be well suited to wall-interference assessment methods based on measured-flow boundary conditions.

ADAPTIVE-WALL METHODS

In an adaptive-wall wind tunnel, the infinite flow past a model in free air is simulated by dividing the flow into two regions: an inner region represented by flow past the model within the test section and an outer region represented mathematically which extends outward from the inner region to infinity. The regions are separated by a contour (or control surface) surrounding the model. The walls of the test section are adjusted so that the inner and outer flow conditions along the contour are compatible.

Linear Iterative Methods

Ferri and Baronti (ref. 1) and Sears (ref. 2) independently developed the first and most widely used method for establishing free-air conditions along the contour. In two dimensions, this method requires measurements of streamwise and vertical flow velocities along the contour. The measured distribution of either component can be used to compute the corresponding free-air, outer-flow solution of the other component. The inner (measured) and outer (computed) distributions of the second component are compared, and the walls are adjusted to reduce differences between them. The process is iterated until satisfactory convergence is achieved.

This two-component adaptive-wall method is most easily applied in test sections with solid but flexible walls. Because the upper and lower walls approximate a contour bounding an infinite strip, streamwise and normal velocity components along the contour are easily deduced (neglecting the displacement effect of the wall boundary layers) from the shapes of the walls and the static pressure distributions along them.

In ventilated test sections, the walls do not form a suitable contour because the flow adjacent to them is generally complex and three-dimensional. Instead, the contour must lie in the inviscid flow between the model and the walls, a region much less accessible to flow measurement instruments.

Davis developed an alternative adaptive-wall method that helps simplify this instrumentation problem (ref. 3). It requires measurements of only one component of velocity (either streamwise or vertical) along two contours surrounding the model. The inner and outer flow regions overlap between the contours. Flow measurements on the inner contour are used to compute the corresponding, free-air distribution of the same component along the outer contour. The walls are adjusted to reduce differences between the inner flow (measured) and outer flow (computed) velocity distributions along the outer contour. As with the two-component method, this method must be iterated.

If the flow in the outer region is subsonic, it can be described by the linear Prandtl-Glauert equation. The free-air relationships for the one- and two-component adaptive-wall methods can then be derived analytically and expressed in closed form. For contours extending upstream and downstream to infinity (i.e., bounding an

infinite strip, figs. 2(a) and 2(b)), the upper and lower outer regions are uncoupled and the free-air relationships along the resulting axial measurement lines are given by:

one-component (ref. 3)

$$u_f(x,y_2) = \frac{\beta|y_2 - y_1|}{\pi} \int_{-\infty}^{\infty} \frac{u_f(\xi,y_1)}{(x - \xi)^2 + \beta^2(y_2 - y_1)^2} \, d\xi \tag{1a}$$

$$w_f(x,y_2) = \frac{\beta|y_2 - y_1|}{\pi} \int_{-\infty}^{\infty} \frac{w_f(\xi,y_1)}{(x - \xi)^2 + \beta^2(y_2 - y_1)^2} \, d\xi \tag{1b}$$

two-component (ref. 2)

$$u_f(x,y) = \frac{1}{\pi\beta} \int_{-\infty}^{\infty} \frac{w_f(\xi,y)}{x - \xi} \, d\xi \tag{2a}$$

$$w_f(x,y) = \frac{-\beta}{\pi} \int_{-\infty}^{\infty} \frac{u_f(\xi,y)}{x - \xi} \, d\xi \tag{2b}$$

To apply these relationships in a real test section, several approximations must be made. (1) In iterative adaptive-wall algorithms, measured velocities are substituted for the free-air velocities in the integrands of equations (1) and (2). Thus we will refer to these as "iterative" methods. (2) Because u is a perturbation quantity, it is estimated by subtracting the assumed free-stream velocity from the measured data. (3) Either the infinite integrals must be truncated or the velocity distributions must be extrapolated beyond the ends of the test section.

Truncation or extrapolation errors can be avoided if the measurement contour is closed within the test section upstream and downstream of the model (fig. 2(c)). For linear flow in the outer region, the free-air relationships between streamwise and vertical perturbation velocities on a closed contour are (refs. 4,5):

$$u_f(x,y) = \frac{1}{\pi\beta} \int_c \frac{[\beta^2(\eta-y)u_f(\xi,\eta) + (\xi-x)w_f(\xi,\eta)]d\xi - [\beta^2(\xi-x)u_f(\xi,\eta) - \beta^2(\eta-y)w_f(\xi,\eta)]d\eta}{(\xi-x)^2 + \beta^2(\eta-y)^2} \tag{3a}$$

$$w_f(x,y)$$

$$= \frac{-\beta}{\pi} \int_c \frac{[(\xi-x)u_f(\xi,\eta) - (\eta-y)w_f(\xi,\eta)]d\xi + [\beta^2(\eta-y)u_f(\xi,\eta) + (x-\xi)w_f(\xi,\eta)]d\eta}{(\xi-x)^2 + \beta^2(\eta-y)^2} \tag{3b}$$

Note that the solutions above and below the model are coupled. These solutions uncouple and reduce to the two-component/infinite-strip relationships (eq. (2)) if the upstream and downstream boundaries are at infinity.

A closed-contour solution for the one-component method has not been developed. However, it would be of limited value because truncation errors with the one-component method are usually small, as we shall demonstrate later.

Linear One-Step Methods

If the inner flow and the outer flow obey linear equations and the model is small, then free-air velocities at the measurement contour can be accurately estimated from measured velocities in one step, thus eliminating the need for iterative wall adjustments. Such one-step methods are exact if the model is infinitely small or if the wall-induced flow is constant within the contour (i.e., if the assumptions of classical wall-interference theory apply).

Lo and Sickles (ref. 6) derived the following one-step solution to the two-component, infinite-strip problem:

$$u_f(x,\pm y) = \frac{1}{2}u(x,\pm y) \pm \frac{1}{2\pi\beta}\int_{-\infty}^{\infty}\frac{w(\xi,\pm y)}{x-\xi}\,d\xi - \frac{\beta y}{2\pi}\int_{-\infty}^{\infty}\frac{u(\xi,\mp y)}{(\xi-x)^2+\beta^2y^2}\,d\xi$$

$$\pm \frac{1}{2\pi\beta}\int_{-\infty}^{\infty}\frac{(\xi-x)w(\xi,\mp y)}{(\xi-x)^2+\beta^2y^2}\,d\xi \tag{4a}$$

$$w_f(x,\pm y) = \frac{1}{2}w(x,\pm y) \mp \frac{\beta}{2\pi}\int_{-\infty}^{\infty}\frac{u(\xi,\pm y)}{x-\xi}\,d\xi - \frac{\beta y}{2\pi}\int_{-\infty}^{\infty}\frac{w(\xi,\mp y)}{(\xi-x)^2+\beta^2y^2}\,d\xi$$

$$\mp \frac{\beta}{2\pi}\int_{-\infty}^{\infty}\frac{(\xi-x)u(\xi,\mp y)}{(\xi-x)^2+\beta^2y^2}\,d\xi \tag{4b}$$

Unlike the iterative solutions, the one-step solutions above and below the model are coupled. Note that all velocities on the right sides of the equations are measured

and that the sum of the first two terms is the average of the measured velocities and the iterative solutions.

On a closed contour, the one-step solution to the two-component problem is the average of the measured velocities and the iterative solutions (eqs. (3a) and (3b)) (refs. 4 and 5).

Free-air upwashes can be computed in one step from measurements of upwash along two contours by extending the one-component correction method described in reference 7. According to this method, wall-induced upwashes along the inner contour can be computed from the upwashes measured along both contours. Subtracting these wall-induced upwashes from the measured upwashes yields the free-air upwashes along the inner contour. The free-air upwashes along the outer contour can then be obtained from equation (1b). This method can also be applied to measurements of streamwise velocities on two infinite contours.

Nonlinear Solutions

Nonlinear effects become significant in the outer flow if the local Mach number exceeds about 0.9. As no analytic solutions exist to the nonlinear problem, an algorithm was developed for approximating the solution to the transonic small perturbation (TSP) equation in the outer region. The outer region above the model was approximated by a rectangular space bounded by the measurement level (for the one-component method the space was bounded by the inner level) and three far-field boundaries (fig. 3). The measured upwash distribution was applied as the boundary condition along the measurement level, and linear theory was used to estimate free-air conditions on the far-field boundaries. The resulting boundary value problem was solved with finite differences as discussed in the "Methods of Solution" section.

CORRECTION METHODS

Since the development of adaptive-wall wind tunnels, engineers have learned to use measured flow boundary conditions to estimate wall-induced velocities near the model. As with classical correction methods, these velocities can then be interpreted as "corrections" to free-stream conditions (ref. 8). The advantage of this approach compared to classical methods is that it eliminates the need to include information about the wall itself in the assessment scheme. The disadvantage is that it requires many flow measurements at or near the wind tunnel walls. However, in an adaptive-wall wind tunnel, this disadvantage is inconsequential because these measurements are also needed to adjust the test section walls. Correction methods are valuable for adaptive-wall test sections because they provide a quantitative measurement of residual wall interference (ref. 9). The correction methods to be

discussed here are based on the assumptions of classical wall-interference theory--the same assumptions discussed earlier in connection with the one-step adaptive-wall methods.

Capelier, Chevallier, and Bouniol (ref. 10) developed the first correction method to exploit measured flow boundary conditions. This method is particularly simple because it requires measurements of only one component of velocity along one contour surrounding the model. The method is derived from the Schwarz Integral Formula (ref. 11) which allows the wall-induced complex velocity field within the contour to be defined, up to a complex constant of integration, by the distribution of either its real or imaginary component along the contour. The wall-induced velocities along the contour are estimated by subtracting free-air velocities caused by the model from the measured velocities. The free-air model-induced velocities are estimated from elementary singularities with strengths set to match the measured forces and moments on the model.

If the contour bounds an infinite strip defined by $-y \leq \eta \leq y$, then the Schwarz formula defines the wall-induced velocities along the tunnel centerline from the symmetric and antisymmetric components of either the wall-induced upwash or streamwise velocity along the contour:

$$w_i(x,0) = \frac{1}{\beta y} \int_{-\infty}^{\infty} \frac{\bar{w}_i(\xi,y)}{2 \cosh[\pi(\xi - x)/2\beta y]} \, d\xi \tag{5a}$$

$$u_i(x,0) = \frac{-1}{\beta^2 y} \int_{-\infty}^{\infty} \frac{\tilde{w}_i(\xi,y)}{e^{-\pi/\beta y(x-\xi)} + 1} \, d\xi + C \tag{5b}$$

$$w_i(x,0) = \frac{1}{y} \int_{-\infty}^{\infty} \frac{\tilde{u}_i(\xi,y)}{e^{-\pi/\beta y(x-\xi)} + 1} \, d\xi + C \tag{5c}$$

$$u_i(x,0) = \frac{1}{\beta y} \int_{-\infty}^{\infty} \frac{\bar{u}_i(\xi,y)}{2 \cosh[\pi(\xi - x)/2\beta y]} \, d\xi \tag{5d}$$

The constants of integration are zero if wall-induced flow perturbations vanish far upstream of the model.

Other one-component/one-contour methods have been developed (ref. 5) but will not be considered here. They are similar to the method described earlier and share its principal disadvantages: having to estimate both the model-induced velocities and a constant of integration. These methods do not fully exploit the information available from adaptive-wall boundary measurements.

If a single component of velocity is measured along a second contour, as required by the one-component adaptive-wall method, then the wall-induced velocities along the inner contour can be computed directly from the measured velocities

without any information about the model (ref. 7). The wall-induced velocities near the model are then easily obtained from the Schwarz formulae (eqs. (5a)-(5d)). This method is directly related to the linear-iterative adaptive-wall method in that it involves a functional of the error function (the differences between measured velocities and the adaptive-wall solution) along the outer contour. Although it eliminates the need to simulate the model, the method retains the uncertainty of the constants of integration in equations (5b) and (5c).

Ashill and Weeks (ref. 12) have shown how wall-induced velocities near the model can be computed from measurements of two components of velocity along a single contour surrounding the model. This method can be derived from the Cauchy Integral Formula (ref. 13) and is particularly elegant because there are no constants of integration to evaluate and it requires no information about the model. If the contour bounds the infinite strip $-y \leq \eta \leq y$, then the wall-induced velocities along the tunnel centerline are given by (ref. 5):

$$u_i(x,0) = \frac{1}{\pi\beta} \int_{-\infty}^{\infty} \frac{(\xi - x)\tilde{w}(\xi,y) + \beta^2 y\bar{u}(\xi,y)}{(\xi - x)^2 + \beta^2 y^2} \, d\xi \tag{6a}$$

$$w_i(x,0) = \frac{-\beta}{\pi} \int_{-\infty}^{\infty} \frac{(\xi - x)\tilde{u}(\xi,y) - y\bar{w}(\xi,y)}{(\xi - x)^2 + \beta^2 y^2} \, d\xi \tag{6b}$$

If two-component measurements are made along a closed contour, the wall-induced velocities are given by:

$$w_i(x,0) = \frac{\beta}{2\pi} \int_c \frac{[(\xi-x)u(\xi,\eta) - \eta w(\xi,\eta)]d\xi + [\beta^2 \eta u(\xi,\eta) + (x-\xi)w(\xi,\eta)]d\eta}{(\xi-x)^2 + \beta^2\eta^2} \tag{7a}$$

$$u_i(x,0) = \frac{-1}{2\pi\beta} \int_c \frac{[\beta^2 \eta u(\xi,\eta) + (\xi-x)w(\xi,\eta)]d\xi - [\beta^2(\xi-x)u(\xi,\eta) - \beta^2\eta w(\xi,\eta)]d\eta}{(\xi-x)^2 + \beta^2\eta^2} \tag{7b}$$

METHODS OF SOLUTION

As part of the present study, computer programs were written to implement each of the adaptive-wall and correction methods described above. Each program processes measured-flow boundary-conditions data in the form in which the data will be generated in the 2- × 2-ft tunnel adaptive-wall test section. These data will be acquired by the laser velocimeter at a set of discrete points along each contour (figs. 4 and 5).

Numerical Integration

All of the integrals were solved by numerical integration. The closed-contour integrals (eqs. (3) and (7)) were evaluated using Everhart's algorithm (ref. 4), which assumes linear variation of velocities between adjacent control points. The assumption of linearly varying velocities was also used to evaluate equations 1, 2, 4, and 6 because, in these cases, its use resulted in integrals that could be evaluated in closed form on each interval. The integrals in eqs. (5a)-(5d) were solved using the trapezoidal rule, which assumes linear variation of the entire integrand between control points.

The two-component adaptive-wall integrals (eqs. (2) and (3)) include singular points. The integrals were evaluated at these points by the limiting procedure described by Everhart (ref. 4).

Extrapolation

The measured velocities in the integrands of the infinite-strip integrals were extrapolated beyond the ends of the test section by one of several methods. The measured velocities in the adaptive-wall integrals were fitted with the velocity distribution caused by six singularities (source, vortex, two doublets, and two quadrupoles) at the model quarter chord (ref. 14). For example, equation (2a) was expressed as:

$$u_f(x,y) = \frac{1}{\pi\beta}\left[\int_{-\infty}^{x_u} \frac{w_s(\xi,y)}{x-\xi}\,d\xi + \int_{x_u}^{x_d} \frac{w(\xi,y)}{x-\xi}\,d\xi + \int_{x_d}^{\infty} \frac{w_s(\xi,y)}{x-\xi}\,d\xi\right]$$

$$= \frac{1}{\pi\beta}\int_{-\infty}^{\infty} \frac{w_s(\xi,y)}{x-\xi}\,d\xi + \frac{1}{\pi\beta}\int_{x_u}^{x_d} \frac{w(\xi,y) - w_s(\xi,y)}{x-\xi}\,d\xi$$

$$= u_s(x,y) + \frac{1}{\pi\beta}\int_{x_u}^{x_d} \frac{w(\xi,y) - w_s(\xi,y)}{x-\xi}\,d\xi$$

where

x_u the most upstream point where velocity is measured

x_d the most downstream point where velocity is measured

w_s the upwash distribution caused by the singularities which gives the best fit of $w(\xi,y)$

u_s the corresponding streamwise perturbation velocity caused by the singularities

The last step is possible because velocity distributions caused by singularities in free air satisfy the free-air relationships (eq. (2a)). Note that the final integral is zero if the singularities provide a perfect fit of the measured data.

In a similar manner, equations (2b), (1a), and (1b) were expressed as:

$$w_f(x,y) = w_s(x,y) - \frac{\beta}{\pi}\int_{x_u}^{x_d} \frac{u(\xi,y) - u_s(\xi,y)}{x - \xi}\, d\xi$$

$$u_f(x,y_2) = u_s(x,y_2) + \frac{\beta|y_2 - y_1|}{\pi}\int_{x_u}^{x_d} \frac{u(\xi,y_1) - u_s(\xi,y_1)}{(x - \xi)^2 + \beta^2(y_2 - y_1)^2}\, d\xi$$

$$w_f(x,y_2) = w_s(x,y_2) + \frac{\beta|y_2 - y_1|}{\pi}\int_{x_u}^{x_d} \frac{w(\xi,y_1) - w_s(\xi,y_1)}{(x - \xi)^2 + \beta^2(y_2 - y_1)^2}\, d\xi$$

The velocities used by the one-component correction methods were extrapolated approximately three tunnel heights beyond the ends of the test section by assuming they decayed in inverse proportion to the absolute distance from the model.

The velocities in the integrands of the two-component correction equations were not extrapolated. The resulting errors were expected to be small because the kernels in equations (6a) and (6b) rapidly become small for large values of $|\xi - x|$.

Nonlinear Adaptive-Wall Method

The TSP equation, expressed in terms of the perturbation velocity potential, can be written (Lottati, I., Implicit, Nonswitching, Vector-Oriented Finite-Difference Algorithms for Steady Transonic Flow Calculation. Unpublished manuscript)

$$(1 - K^2)\frac{\partial^2\phi}{\partial x^2} + \frac{\partial^2\phi}{\partial y^2} = 0$$

where

$$K^2 = M_\infty^2\left[1 + (\gamma + 1)\frac{\partial\phi}{\partial x}\right]$$

The solution to this equation was approximated by the method of finite differences. The terms $\partial^2\phi/\partial y^2$ and $\partial\phi/\partial x$ were represented by second-order-accurate central-difference operators throughout the computational domain. The term $\partial^2\phi/\partial x^2$ was approximated by a central-difference operator at mesh points where $M < 1.0$ and by a second-order upwind-difference operator at points where $M \geq 1.0$. No special

shock-point operator was used (i.e., the solutions were not fully conservative (ref. 15)).

Neumann boundary conditions were applied to all four sides of the rectangular domain (fig. 3). The boundary condition along the measurement line, $y = y_1$, was the upwash distribution measured there. Boundary conditions along the upper boundary, $y = y_{ff}$, were estimated from the measured upwashes using equation (1b). Finally, at the upstream and downstream boundaries, $\partial\phi/\partial n = u$ was estimated from the measured upwash distribution at $y = y_1$ using equations (1a) and (2a):

$$u(x_{ff},y) = \frac{\beta|y - y_1|}{\pi} \int_{-\infty}^{\infty} \frac{u(\xi,y_1)}{(x_{ff} - \xi)^2 + \beta^2(y - y_1)^2} d\xi$$

where

$$u(\xi,y_1) = \frac{1}{\pi\beta} \int_{-\infty}^{\infty} \frac{w(\xi',y_1)}{\xi - \xi'} d\xi'$$

The solutions to the difference equations were approximated iteratively, row by row, sweeping outward from the lower boundary.

TEST CASES

The adaptive-wall and correction methods were applied to simulated wind tunnel data. These data were generated by two methods. In the first and simplest method, a lifting airfoil with thickness in free air was represented by a vortex and doublet at $x/c = 0.25$ and $y = 0$. Solid-wall boundary conditions could be added by superimposing a system of image singularities at $x/c = 0.25$ and $y = \pm n(h/2)$ where n is an integer. This representation is convenient because it exactly satisfies the assumptions of classical wall-interference theory and the model- and wall-induced velocities are easily separated.

Wind tunnel data were also simulated using the computer program TSFOIL (ref. 16). This program solves the TSP equations for flow past an airfoil subject to free-air conditions or any of several other wall boundary conditions. The program was modified to output streamwise and vertical perturbation velocities at control points specified by the user (Byerly, J., private communication). The TSFOIL simulations provided a check of the adaptive-wall and correction methods in transonic flows in which nonlinear effects are present.

For both types of flow simulations, perturbation velocities were computed at the points where flow measurements will be made in the Two- by Two-Foot Wind Tunnel (figs. 4 and 5). The control points along each axial line were centered with respect to the plenum compartments to facilitate wall-adjustment calculations.

The test cases were used to assess the accuracies of the methods and to study their sensitivities to (1) uncertainties in free-stream conditions and (2) errors in

extrapolating velocities beyond the ends of the test section. In figures 6-15, solutions computed by the adaptive-wall and correction methods are compared with simulated data along axial lines in the test section. Table 1 summarizes the flow conditions of each simulation along with the type of method applied and the relevant equation and reference numbers.

Adaptive-Wall Methods

Test case (1). A vortex and doublet in free air ($M_\infty = 0.5$, $C_\ell = 0.4$, $A = 0.4$)- Free-air data should exactly satisfy the iterative adaptive-wall relationships (eqs. (1) and (2)). Figures 6(a) through 6(f) compare data for a vortex and doublet in free air with outer-flow solutions computed using each of the linear iterative adaptive-wall relationships. In each case, the outer-flow solution is very accurate.

Note from figure 6 that significant velocity perturbations persist at the ends of the test section. Thus, the infinite-strip methods can be expected to be sensitive to extrapolation errors. To point out this sensitivity, figures 6(a) through 6(d) include the outer solutions that were obtained by truncating the infinite integrals at the most upstream and downstream measurement locations.

The contributions of the truncated velocity distributions to the one-component solutions are small except at the extreme stations (figs. 6(a) and 6(b)). This makes sense because the kernels in equations (1a) and (1b) rapidly become small as $|x - \xi|$ increases. The two-component solution for w (fig. 6(c)) is also altered only slightly by truncating the integral (eq. (2b)). This occurs because the sign of the integrand upstream of the model is opposite from the sign downstream; thus the contributions of the upstream and downstream truncated regions approximately cancel each other. On the other hand, the two-component solution for u (fig. 6(d)) changes significantly if the infinite integral (eq. (2a)) is truncated. This occurs because the kernel in equation (2a) does not decrease as rapidly as the one-component kernels for large $|\xi - x|$ and because the integrand has the same sign upstream and downstream of the model so the truncated regions add to the total.

The two-component, infinite-strip boundary data can also be analyzed by the two-component, closed-contour method by interpolating velocity data across the ends of the test section. Figures 6(e) and 6(f) compare solutions obtained in this way with the closed contour solutions obtained by including data along these boundaries. The differences between the solutions are quite small.

As all of the solutions discussed so far are expressed in terms of velocity perturbations, the exact direction and magnitude of the free-stream vector is assumed to be known. However, because significant model-induced flow perturbations occur everywhere in the test section, free-stream conditions cannot be measured directly. To illustrate the effects of uncertainty in the free-stream vector, outer solutions were computed for the vortex and doublet in free air with the Mach number in the data reduction assumed to be 0.005 less than the true Mach number, as shown

in figure 7. Likewise, figure 8 illustrates outer solutions for which the true and assumed directions of the free stream differed by 0.1°.

The one-component methods indicate interference-free flow even when erroneous free-stream conditions are assumed (figs. 7(a), 7(b), 8(a), and 8(b)). Thus they are of little use in establishing free-stream conditions. This result is not surprising because velocity measurements on both contours are equally affected by the error. However, the two-component solutions (figs. 7(c), 7(d), 8(c), and 8(d)) differ from the measured data when erroneous free-stream conditions are assumed because the normal and streamwise perturbation velocities are not equally affected by errors in the free-stream quantities and both are involved in the interference assessment. Specifically, u is very sensitive to errors in U whereas w is not. Likewise, w is sensitive to errors in the free-stream direction whereas u is not. Therefore, boundary data which satisfy the two-component free-air relationships also establish free-stream conditions without any additional measurements.

Test case (2). A vortex and doublet in a solid-wall tunnel ($M_\infty = 0.5$, $C_\ell = 0.4$, $A = 0.4$)- Consider the same vortex and doublet combination, but in a solid-wall wind tunnel instead of free air. Figures 9(a) through 9(f) show the solid-wall velocity distributions along with the iterative and one-step outer solutions computed from the solid-wall data. The velocities caused by the singularities in free air are also shown. Note that each one-step solution agrees quite well with the free-air data.

A comparison of one- and two-component iterative solutions shows that the apparent error (the difference between the solid-wall data and the iterative solutions) is much greater using the two-component method. Thus the two-component method is more sensitive to wall interference. The sensitivity of the one-component method can be increased by increasing the separation between the inner and outer contours. Maximum sensitivity, which occurs when the outer contour is at the wall and the inner contour is very close to the model, is difficult to achieve in practice, especially in a wind tunnel with ventilated walls, for two reasons: (1) flow at the walls tends to be complex and three dimensional, and (2) flow near the model may be separated or include strong shock waves. The sensitivity of the two-component method is nearly independent of the location of the single contour.

The one-component iterative solutions lie between the solid-wall and free-air data (figs. 9(a) and 9(b)), which implies that iterative wall adjustments computed from the one-component data should be overrelaxed. In contrast, the two-component iterative solutions (figs. 9(c) through 9(f)) would generate larger velocity changes than are really required. Thus, the two-component, iterative wall-control algorithms should be underrelaxed.

Test case (3). NACA 0012 airfoil in free air ($M_\infty = 0.80$, $\alpha = 2.0°$)- This test case illustrates the importance of accounting for nonlinear effects whenever velocities in the outer flow approach the speed of sound. The TSFOIL program was used to simulate flow past an NACA 0012 airfoil in free air at $M_\infty = 0.80$ and $\alpha = 2.0°$.

At these conditions, the maximum Mach numbers along the inner (y/c = 1.0) and outer (y/c = 1.5) contours are 1.015 and 0.919, respectively.

In figure 10 the free-air data and the linear, iterative outer flow solutions are compared. Below the airfoil, where the flow in the outer region is subcritical everywhere, the one-component, linear solutions are quite accurate. Although the two-component solutions predict the correct trends, they are slightly displaced from the free-air data. In the upper outer-flow, linear theory is adequate except for the area immediately above the airfoil.

Figures 10(a) and 10(d) include outer solutions computed using the TSP finite-difference algorithm. The domain for these calculations was limited to the region $-1.0 < x/c < 2.0$ where linear solutions were inaccurate. The upper far-field boundary was $y/c = 3.5$. The TSP solutions are substantially more accurate than the linear solutions in this domain. Both solutions are automatically matched along the boundaries of the TSP domain because linear theory is used in the TSP algorithm to establish boundary conditions. This is a good example of a situation in which linear and nonlinear solutions can be "patched" together to yield an accurate overall solution.

Test case (4). NACA 0012 airfoil in free air ($M_\infty = 0.90$, $\alpha = 0°$)- As a final example of adaptive-wall methods, consider an NACA 0012 airfoil in free air at $M_\infty = 0.90$ and $\alpha = 0°$. In this case the supersonic bubble extends well out into the outer region: the maximum Mach numbers at $y/c = 1.0$ and 1.5 are 1.22 and 1.12, respectively. The linear solutions are somewhat inaccurate near the airfoil where perturbation velocities are greatest (fig. 11). The use of TSP rather than linear theory improves the accuracy of the outer solutions; however, significant errors persist, especially in the two-component solution. The residual errors are probably due to the relatively coarse mesh used in the TSP outer solutions compared to that used in TSFOIL. Unlike the previous example, the domain for these TSP calculations was the entire length of the test section.

Correction Methods

Test case (1). Vortex and doublet in a solid-wall tunnel ($M_\infty = 0.5$, $C_\ell = 0.4$, $A = 0.4$)- All of the correction methods were applied to the boundary data for the vortex and doublet in a solid-wall wind tunnel. These are good data for a test case because the true wall-induced velocities can be determined explicitly from the system of image singularities.

As a rule, the one-component methods accurately predict the component of wall-induced velocity that is parallel to the measured component (figs. 12(a)-12(d)). However, solutions for the perpendicular components tend to be offset from the true solutions because of errors in extrapolating velocities downstream of the test section. Equations 5(b) and 5(c) are particularly sensitive to such errors because the kernels do not approach zero for large values of $x - \xi$. The effects of

extrapolation errors are clearly shown in figs. 12(a) through 12(d) which include solutions obtained without extrapolation.

The agreement between the true solution and the interference velocities computed by the two-component methods (infinite-strip and closed-contour) is quite good (figs. 12(e) and 12(f)). The infinite-strip solution for the wall-induced upwash is offset slightly because of truncation of the infinite integral (eq. (6b)) at the ends of the test section.

Test case (2). Vortex and doublet in free air ($M_\infty = 0.5$, $C_\ell = 0.4$, $A = 0.4$)- When applied to boundary data acquired in free air, the correction methods should predict that wall-induced velocities vanish. This "null test" was applied to the vortex and doublet in free air (fig. 13, solid curves). The solution that deviates most from zero is the one for upwash computed by the two-component/infinite-strip method (fig. 13(e)). Such deviations, largest at the ends of the test section, are due to truncation of the infinite integrals in equation (6b).

Figure 13 also includes interference velocities computed from the same free-air data except that in one case (indicated by dotted curves), the assumed free-stream Mach number was 0.005 less than the true Mach number and in a second case (indicated by the dot-dashed line), the true and assumed free-stream flow angles differed by 0.1°. The two-component/closed-contour solution (fig. 13(f)) gives the clearest interpretation of these errors: the Mach number error becomes a uniform, wall-induced Mach number perturbation equal to the difference between the assumed and true Mach numbers. Likewise, the flow angle error is interpreted as uniform wall-induced upwash. The two-component/infinite-strip method (fig. 13(e)) yields a similar result except that truncation errors make the interpretation more difficult. The one-component methods yield the "correct" interpretation of the component of the wall-induced velocity parallel to the measured component but the solutions for the perpendicular components are inconsistent. The one-component/two-contour solutions (figs. 13(a) and 13(b)) are unreliable since they are deduced from error functions (differences between the measured velocities and the outer solutions illustrated in figs. 7(a), 7(b), 8(a), and 8(b)) that are far too small to be resolved in a real wind tunnel.

Test case (3). NACA 0012 airfoil in free air ($M_\infty = 0.80$, $\alpha = 2°$)- Consider a more realistic configuration: an NACA 0012 airfoil in free air at $M_\infty = 0.80$ and $\alpha = 2.0°$ (fig. 14). As in the previous example, the correct solution for this case is zero wall-induced perturbations. The interference velocities computed by the two-component/closed-contour method are very small: Mach number perturbations near the model do not exceed 0.001, and flow angle perturbations are less than 0.03°. The two-component/infinite-strip method also predicts Mach number perturbations quite accurately but truncation errors are evident in the solution for wall-induced flow angle. The one-component/two-contour solutions for both wall-induced Mach number and flow angle are less accurate than the two-component solutions. The wall-induced upwash computed from streamwise velocity measurements is displaced because of truncation errors. The other errors in the one-component/two-contour solutions

are due to the nonlinear effects that are evident in the adaptive-wall solutions for the same case (fig. 10).

The one-component/one-contour solutions are grossly in error because of nonlinear effects and because singularities at the model quarter-chord did not accurately represent model-induced velocity perturbations along the contour. Greater accuracy could probably have been achieved if the model had been represented by distributed singularities (ref. 17).

Test case (4). NACA 0012 airfoil in a porous-wall tunnel ($M_\infty = 0.80$, $\alpha = 2°$).- The final example is for an NACA 0012 airfoil at $M_\infty = 0.80$ and $\alpha = 2.0°$ in a porous-wall wind tunnel with height-to-chord ratio of 4.0. An exact solution to the wall-induced velocity field does not exist since the model is of finite size and the flow is transonic. Based on the previous examples, however, we expect the two-component/closed-contour solution to be the most reliable.

Differences between the two-component closed-contour and infinite-strip solutions near the model are very small (fig. 15). Although the one-component solutions exhibit the same trends as the two-component methods, the magnitudes of the wall-induced velocities differ significantly. Again, likely reasons for these differences are extrapolation errors, nonlinear effects, and the uncertainty of constants of integration in equations (5b) and (5c). Since the TSFOIL solution is computed in a finite domain, upstream boundary conditions are only approximate and wall-induced perturbations do not necessarily vanish at upstream infinity as assumed by the one-component correction methods.

CONCLUSIONS

Because a two-component laser velocimeter will be available to make the required boundary measurements, the two-component methods appear to be best both for determining wall adjustments and for computing corrections for wall interference in the Two- by Two-Foot Wind Tunnel. Based on the parameter studies that have been discussed, the two-component methods have the following advantages over the one-component method:

1. They are more sensitive to wall interference.

2. They are more sensitive to errors in the direction and magnitude of the free stream. Thus they can be used to establish free-stream conditions without auxiliary measurements.

3. Flow measurements are required at fewer locations, thus significantly reducing data acquisition time.

4. Two-component correction methods are independent of arbitrary constants of integration and a description of the model.

5. Two-component boundary data can be used to predict free-air distributions of both components of velocity thus providing more complete interference information.

A disadvantage of the two-component, infinite-strip, adaptive-wall method is its sensitivity to extrapolation errors. However, these errors can be eliminated entirely by measuring boundary data along a closed contour, which could be easily accomplished with the laser velocimeter.

Linear adaptive-wall methods are accurate if the maximum Mach number in the outer flow does not exceed 0.9. At higher Mach numbers, finite-difference solutions to the TSP equations are significantly more accurate than solutions based on linear theory, both for one- and two-component methods.

REFERENCES

1. Ferri, A.; and Baronti, P.: A Method for Transonic Wind Tunnel Corrections. AIAA J., vol. 11, no. 1, Jan. 1973, pp. 63-66.

2. Sears, W. R.: Self-Correcting Wind Tunnels. Calspan Report no. RK-5070-A-2, July 1973; also Aeronaut. J., vol. 78, Feb.-Mar. 1974, pp. 80-89.

3. Davis, S. S.: A Compatibility Assessment Method for Adaptive-Wall Wind Tunnels. AIAA J., vol. 19, Sept. 1981, pp. 1169-1173.

4. Everhart, J. L.: A Method for Modifying Two-Dimensional Adaptive Wind-Tunnel Walls Including Analytical and Experimental Verification. NASA TP-2081, Feb. 1983.

5. Mokry, M.; Chan, Y. Y.; and Jones, D. J.: Two-Dimensional Wind Tunnel Wall Interference. AGARDograph no. 281, Nov. 1983.

6. Lo, C. F.; and Sickles, W. L.: A Hybrid Method of Transonic Computation with Application to the Adaptive Wind Tunnel. Eighth U.S. National Congress of Applied Mechanics, Los Angeles, Calif., June 26-30, 1978.

7. Schairer, E. T.: Two-Dimensional Wind-Tunnel Interference from Measurements on Two Contours. J. Aircraft, vol. 21, no. 6, June 1984, pp. 414-419.

8. Garner, H. C.; Rogers, E. W. E.; Acum, W. E. A.; and Maskell, E. C.: Subsonic Wind Tunnel Wall Corrections. AGARDograph 109, Oct. 1966.

9. Davis, S. S.: Generalized Adaptive-Wall Wind Tunnels. J. Aircraft, vol. 23, no. 2, Feb. 1986, pp. 158-160.

10. Capelier, C.; Chevallier, J. P.; and Bouniol, F.: Nouvelle Methode de Correction des Effects de Parois en Courant Plan. La Recherche Aerospatiale, Jan.-Feb. 1978, pp. 1-11.

11. Levinson, N.; and Redheffer, R.: Complex Variables. Holden-Day Inc., San Francisco, Calif., 1970, pp. 358-359.

12. Ashill, P. R.; and Weeks, D. J.: An Experimental Investigation of the Drag of Thick Supercritical Aerofoils--A Progress Report. TM Aero 1765, Royal Aircraft Establishment, 1978.

13. Churchill, R. V.: Complex Variables and Applications. McGraw-Hill Book Company, New York, 1960, pp. 118-119.

14. Erickson, J. C., Jr.; and Nenni, J. P.: A Numerical Demonstration of the Establishment of Unconfined-Flow Conditions in a Self-Correcting Wind Tunnel.

15. Murman, E. M.: Analysis of Embedded Shock Waves Calculated by Relaxation Methods. AIAA J., vol. 12, no. 5, May 1974, pp. 626-633.

16. Stahara, S. S.: Operational Manual for Two-Dimensional Transonic Code TSFOIL. NASA CR-3064, Dec. 1978.

17. Smith, J.: A Method for Determining 2D Wall Interference on an Aerofoil from Measured Pressure Distributions near the Walls and on the Model. Nationaal Lucht-en Ruimtevaartlaboratorium TR-810160, Jan. 1981.

TABLE 1.- SUMMARY OF TEST CASES

Fig. No.	Flow condition	Method	Eq. No.	Ref. No.
6	Vortex and doublet in free air $M_\infty = 0.5$, $C_\ell = 0.4$, $A = 0.4$	Adaptive-wall linear/iterative showing truncation errors	1,2,3	1,2,3,4
7		Adaptive-wall linear/iterative showing effect of Mach-No. error		
8		Adaptive-wall linear/iterative showing effect of flow-angle error		
9	Vortex and doublet in solid-wall tunnel $h/c = 0.4$ $M_\infty = 0.5$, $C_\ell = 0.4$, $A = 0.4$	Adaptive-wall one-step	4	6,7
10	NACA 0012 in free air $M_\infty = 0.8$, $\alpha = 2°$	Adaptive-wall linear and TSP	1,2	1,2,3
11	NACA 0012 in free air $M_\infty = 0.9$, $\alpha = 0°$	Adaptive-wall linear and TSP	1,2	1,2,3
12	Vortex and doublet in solid-wall tunnel $h/c = 0.4$ $M_\infty = 0.5$, $C_\ell = 0.4$, $A = 0.4$	Correction showing effect of truncation errors	5,6,7	5,7,10,12
13	Vortex and doublet in free air $M_\infty = 0.5$, $C_\ell = 0.4$, $A = 0.4$	Correction showing effects of Mach-No. and flow-angle errors		
14	NACA 0012 in free air $M_\infty = 0.8$, $\alpha = 2°$	Correction		
15	NACA 0012 in porous-wall tunnel, $h/c = 4.0$ $M_\infty = 0.8$, $\alpha = 2°$	Correction		

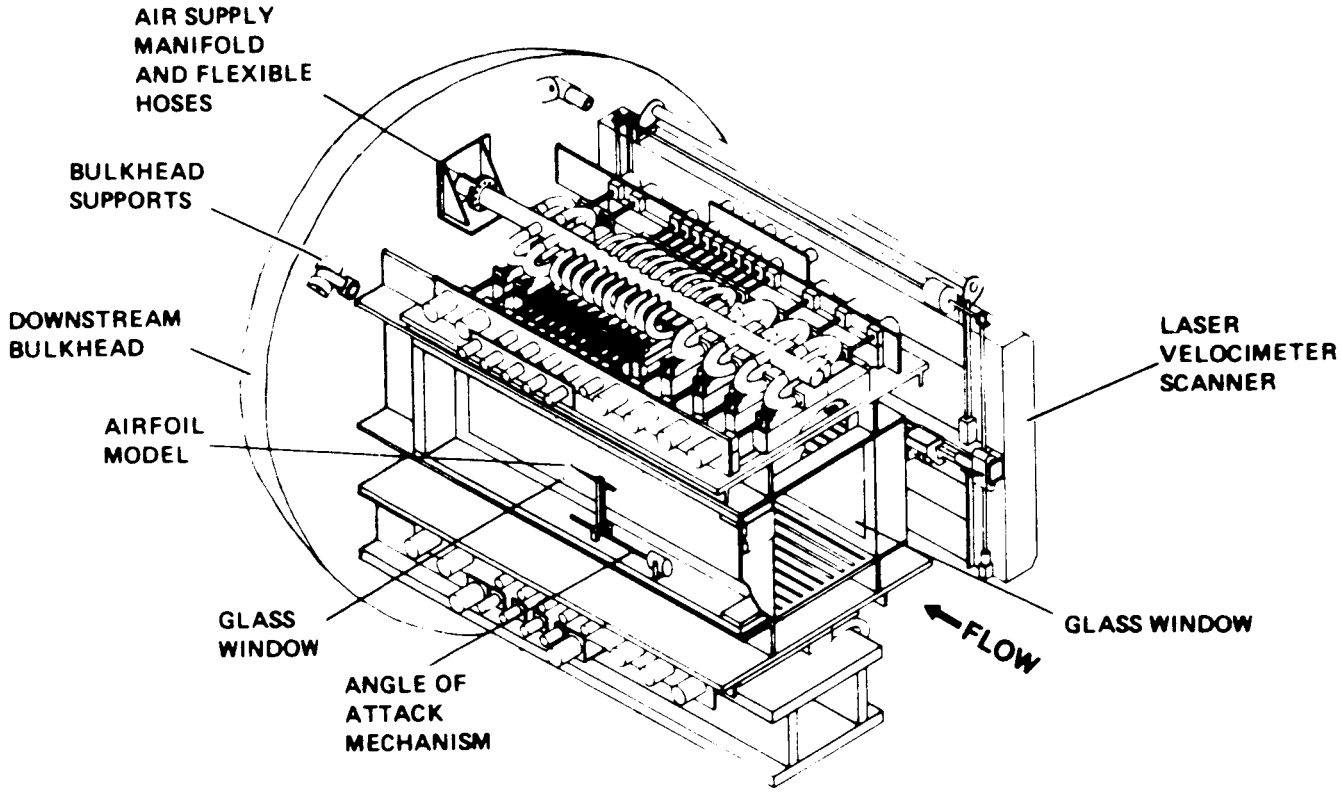

Figure 1.- Schematic of the Two- by Two-Foot adaptive-wall test section.

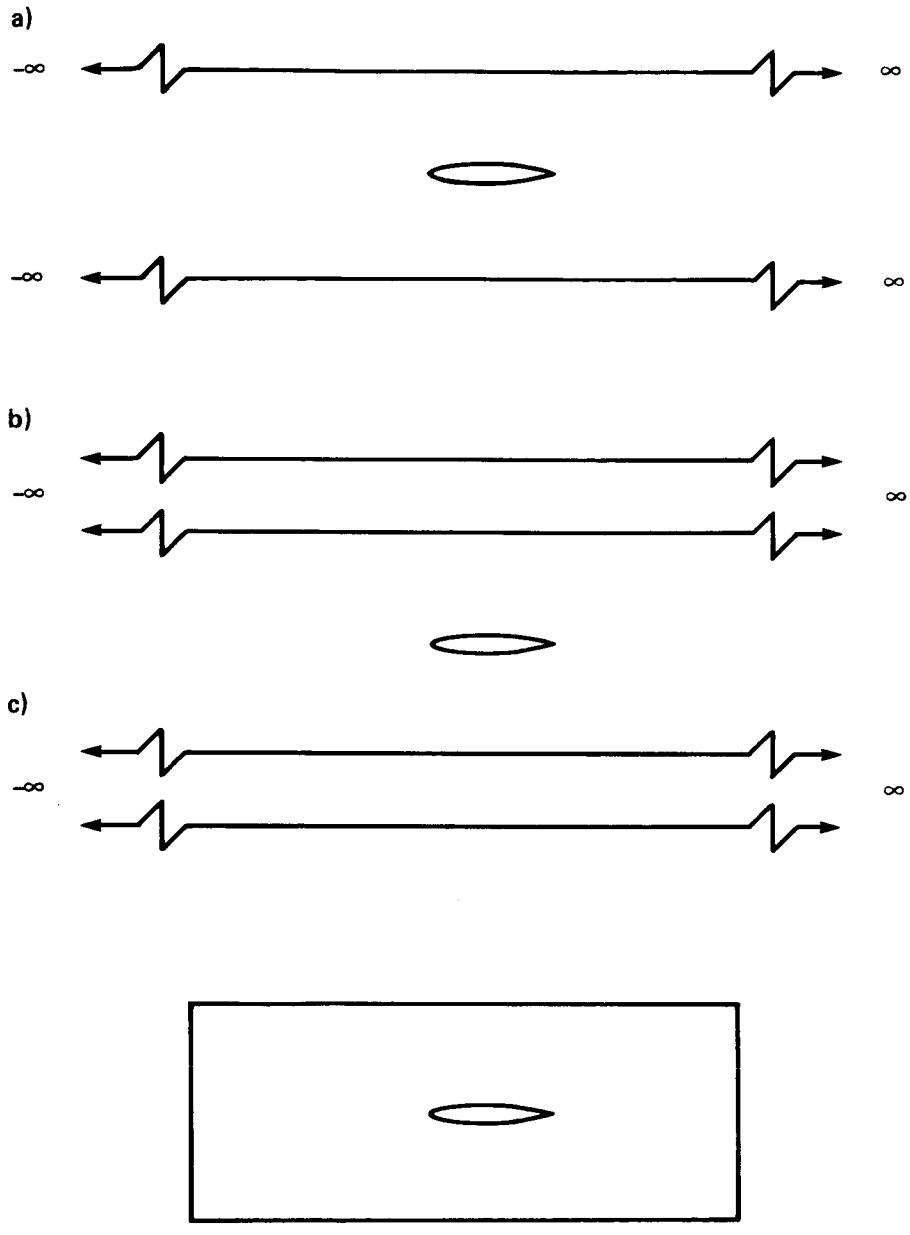

Figure 2.- Control contours for adaptive-wall methods. (a) Two-component/infinite-strip. (b) One-component/infinite-strip. (c) Two-component/closed contour.

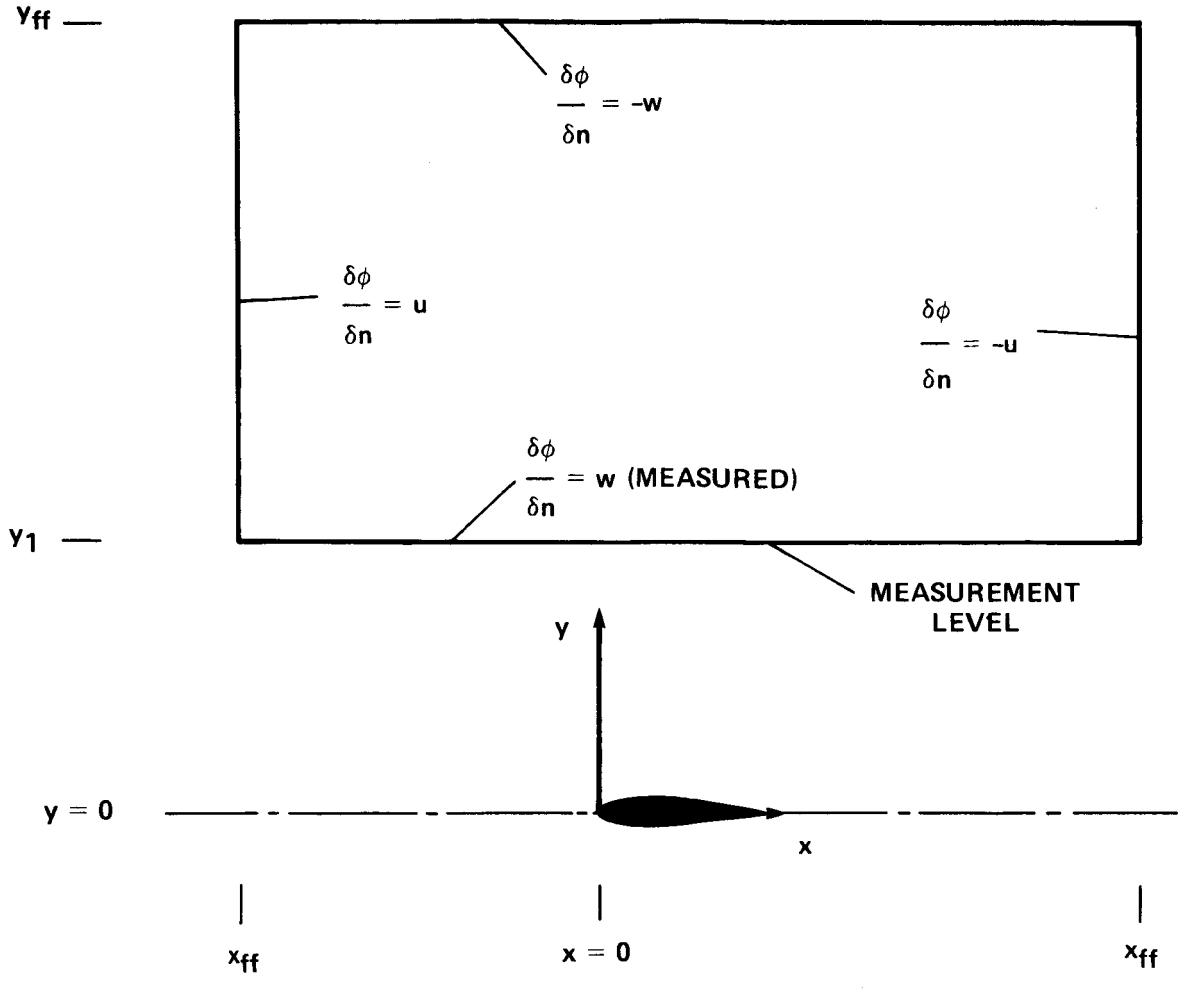

Figure 3.- Domain for the TSP outer-flow calculations.

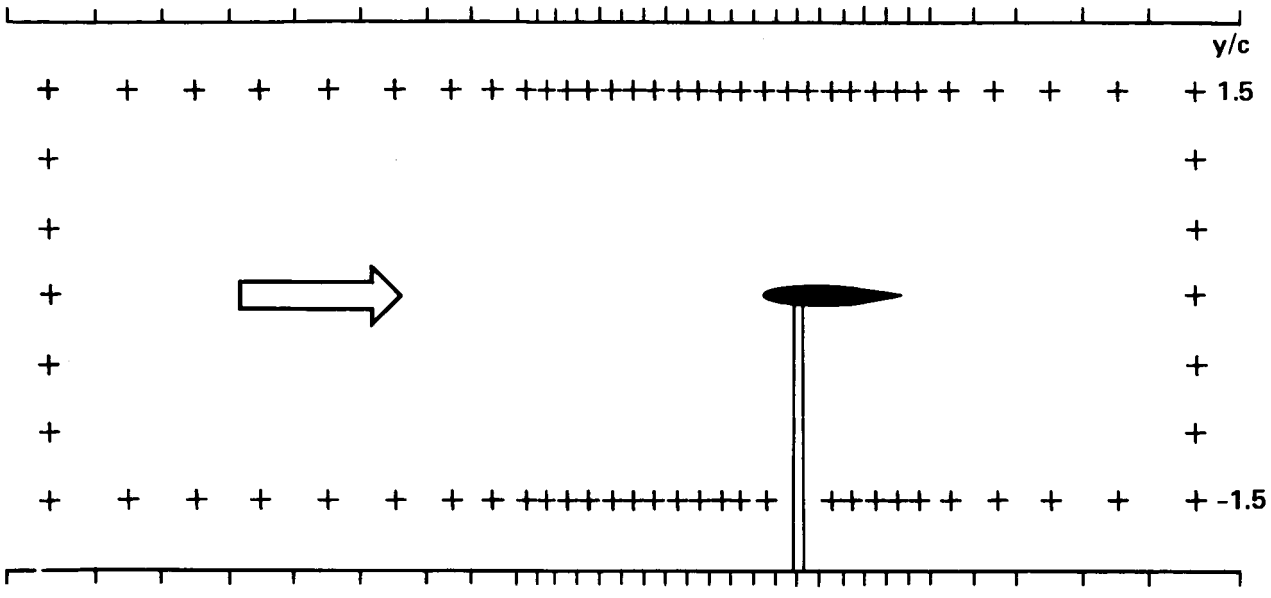

Figure 4.- Side view of the test section showing plenum compartments and laser velocimeter (LV) measurement locations for the two-component methods.

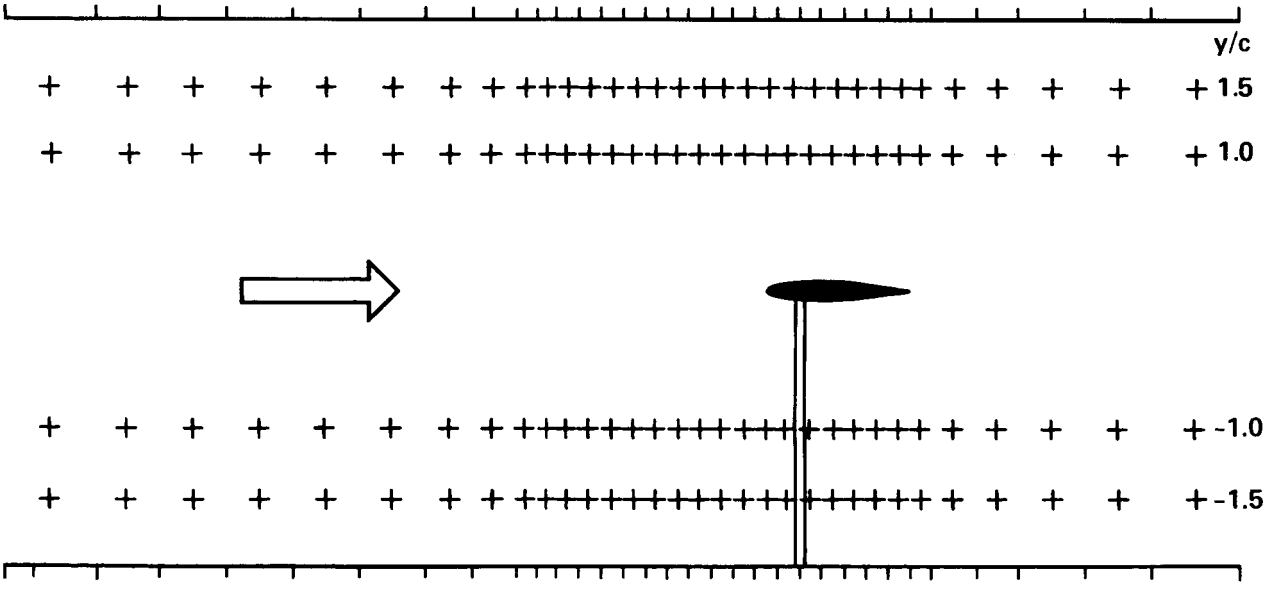

Figure 5.- Side view of the test section showing plenum compartments and LV measurement locations for the one-component/two-contour methods.

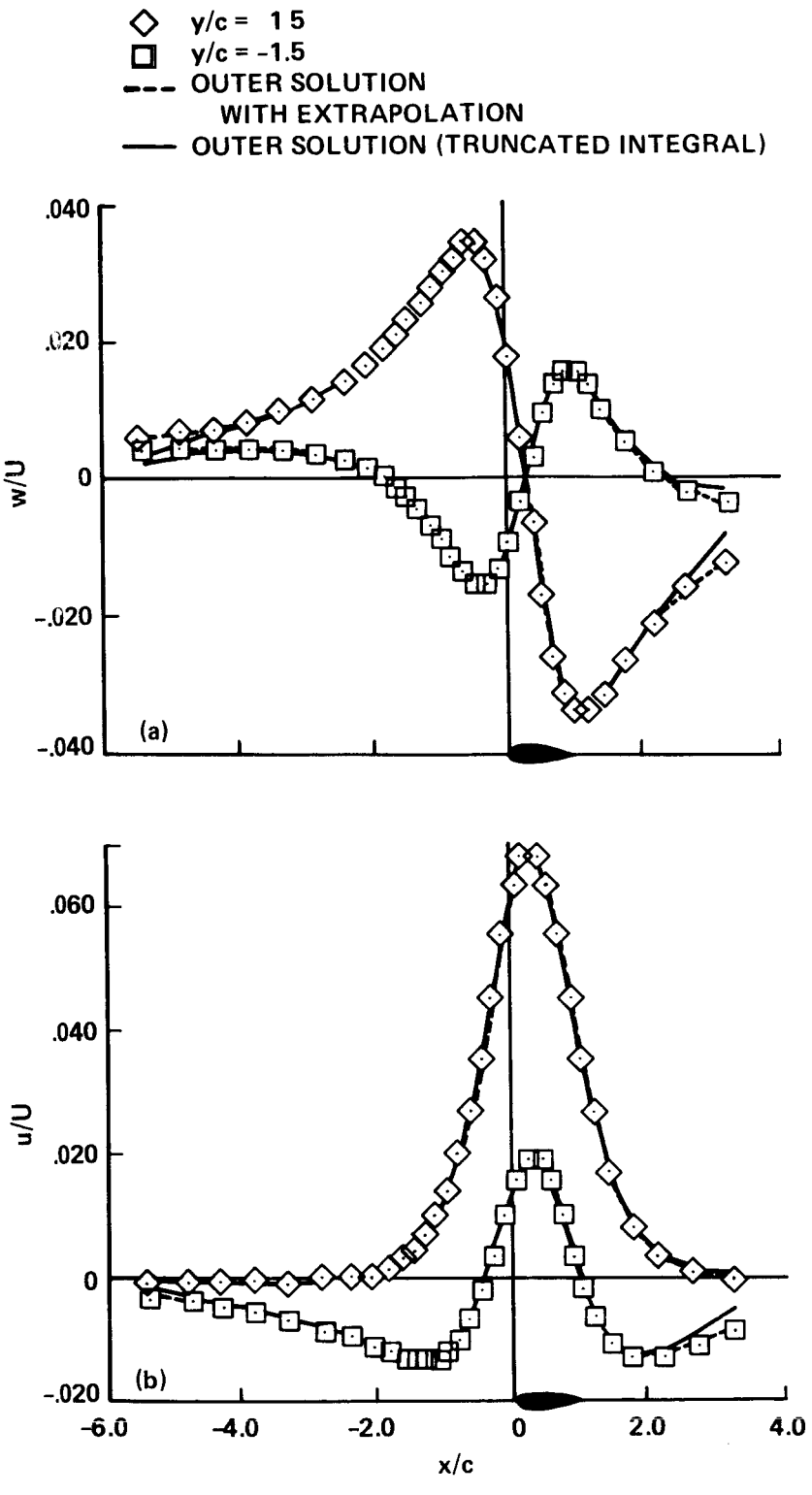

(a) One-component, upwash.

(b) One-component, streamwise.

Figure 6.- Linear, iterative adaptive-wall solutions for a vortex and doublet in free air (M_∞ = 0.50, C_ℓ = 0.4, A = 0.4).

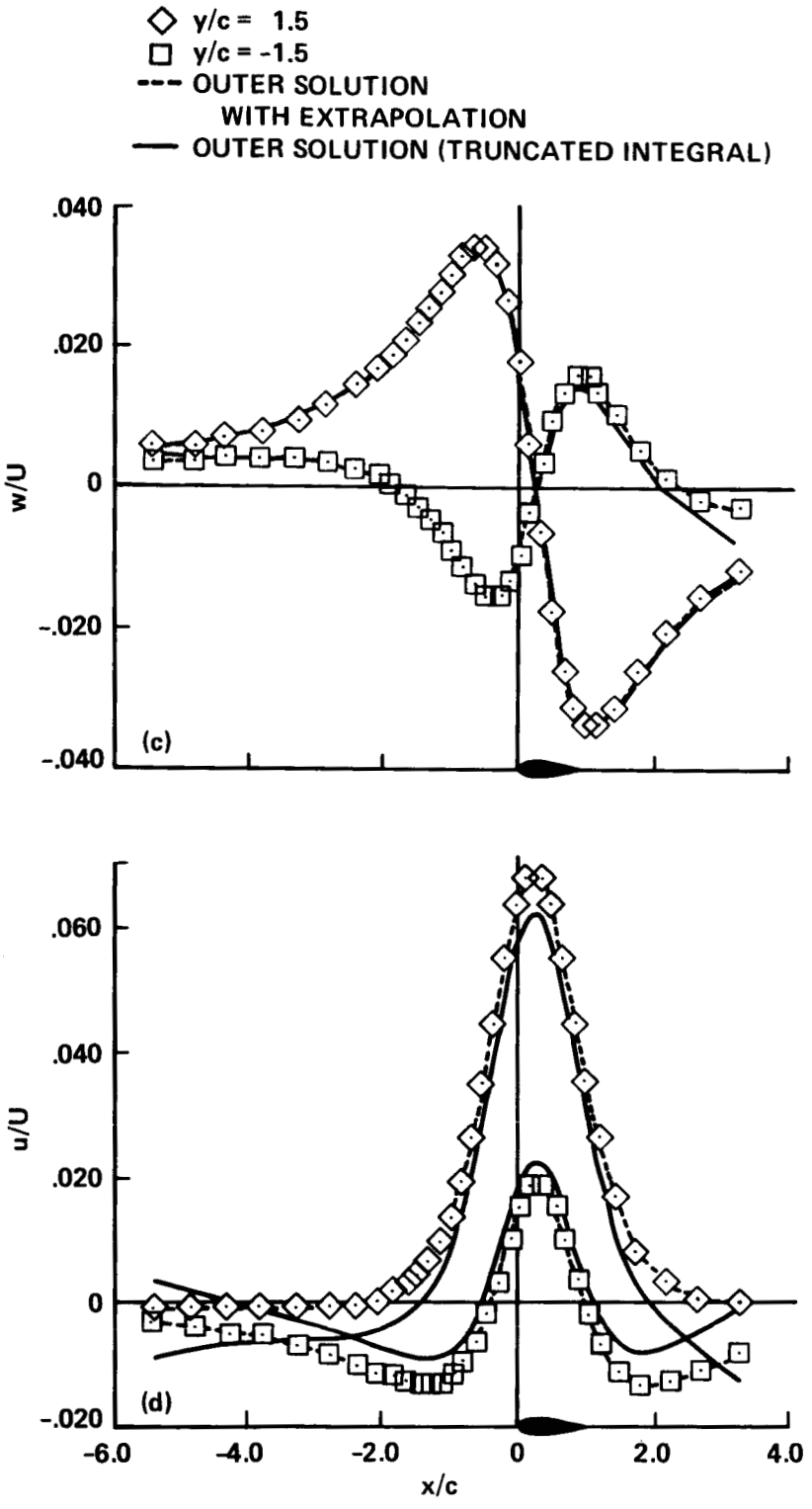

(c) Two-component/infinite-strip, upwash.

(d) Two-component/infinite-strip, streamwise.

Figure 6.- Continued.

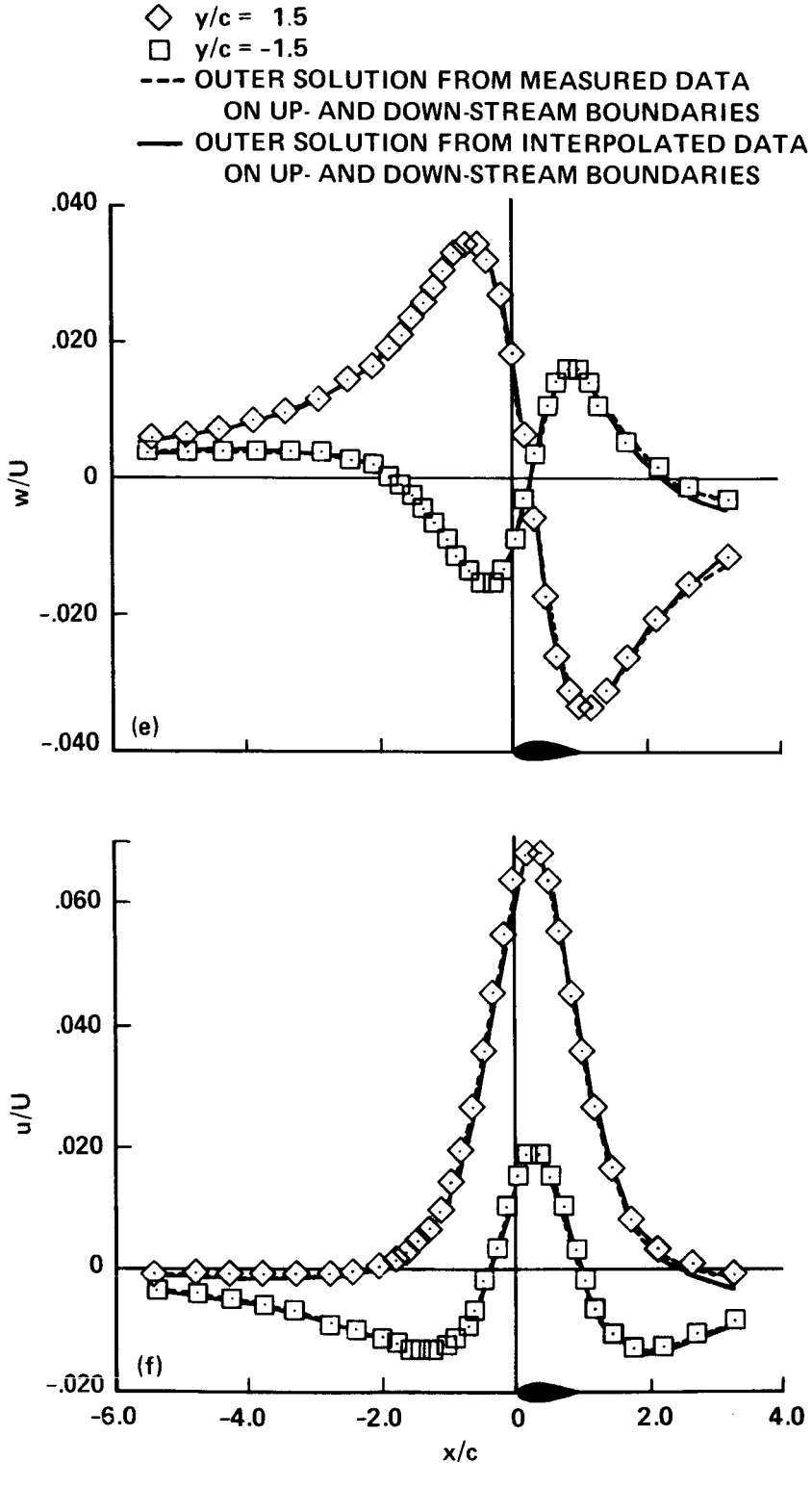

(e) Two-component/closed-contour, upwash.

(f) Two-component/closed-contour, streamwise.

Figure 6.- Concluded.

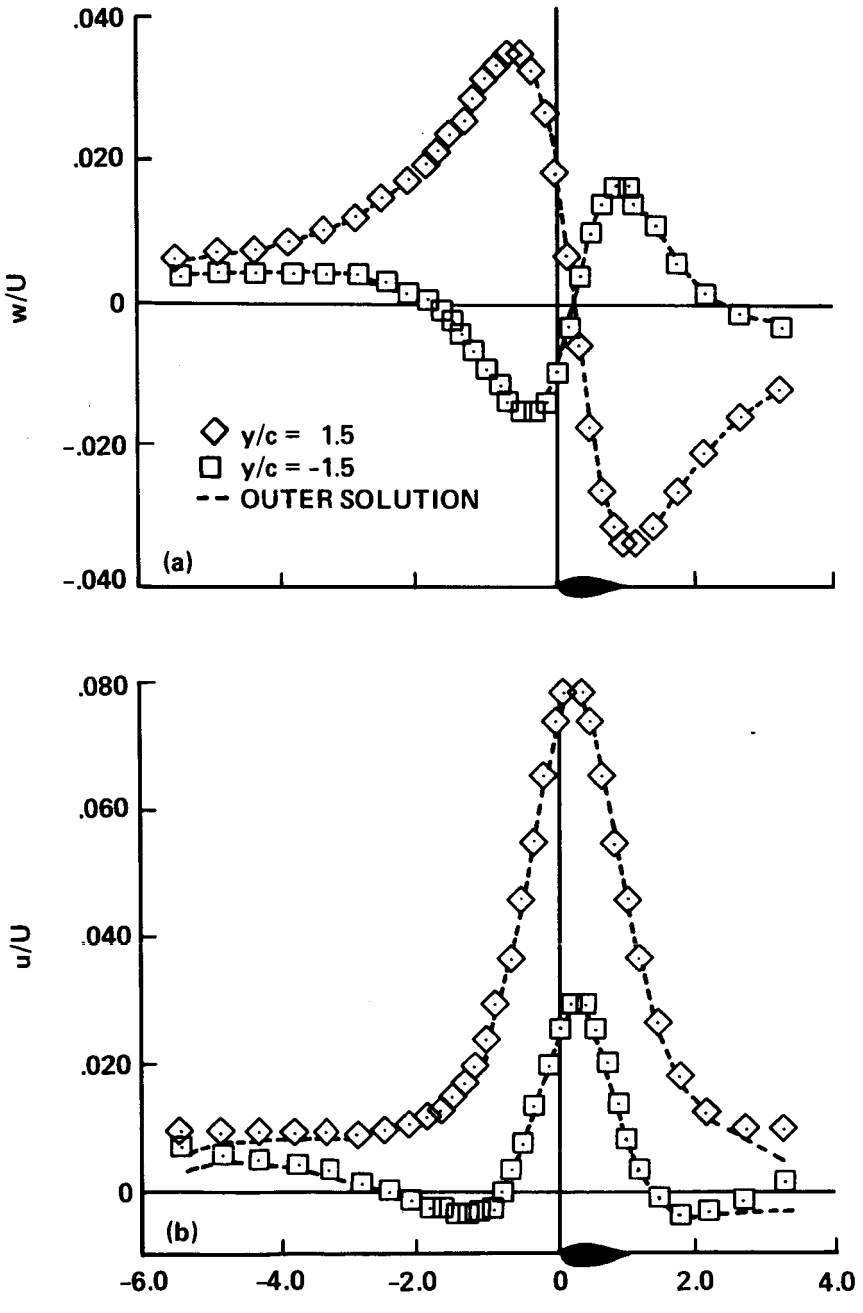

(a) One-component, upwash.

(b) One-component, streamwise.

Figure 7.- Effect of 0.005 Mach number error on adaptive-wall solutions for a vortex and doublet in free air (M_∞ = 0.50, C_ℓ = 0.4, A = 0.4).

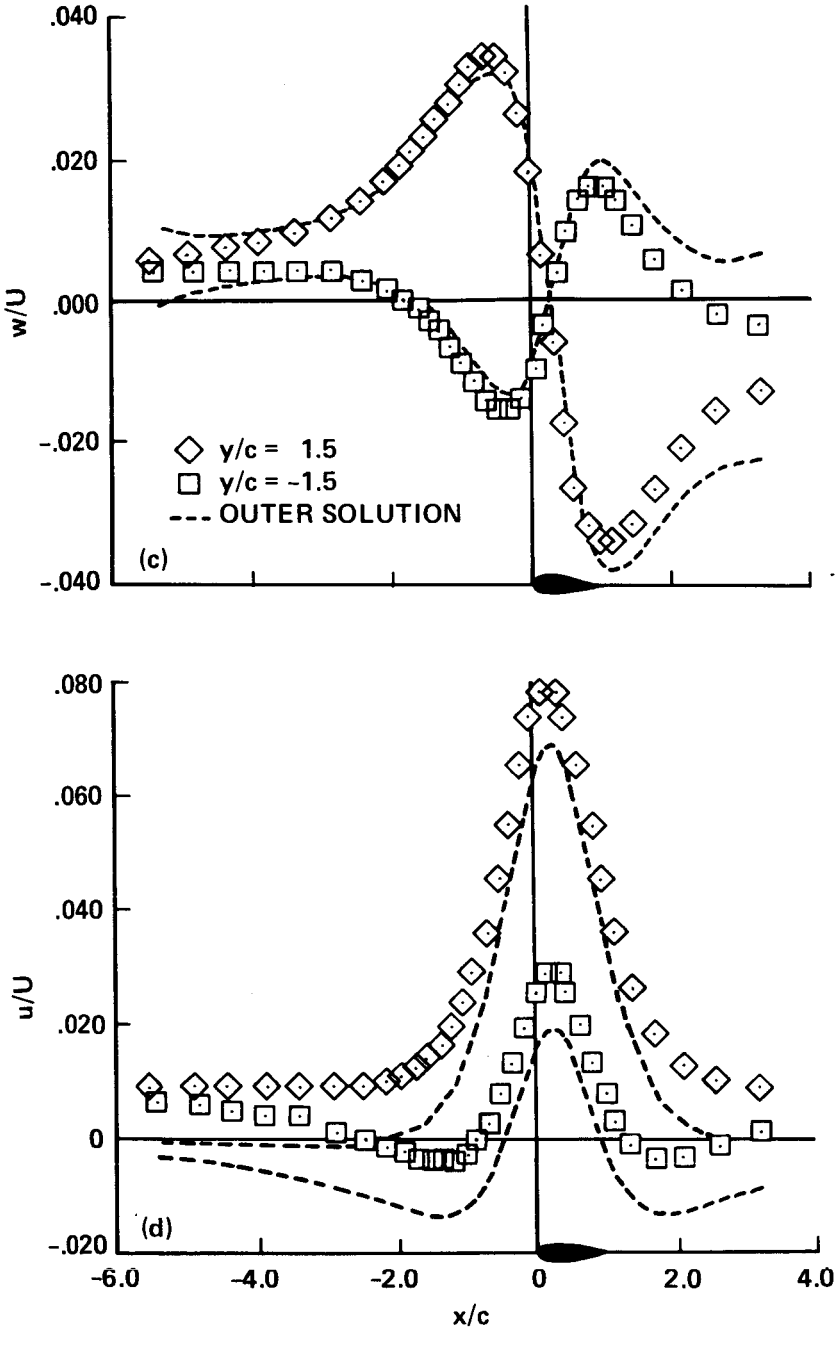

(c) Two-component/infinite-strip, upwash.

(d) Two-component/infinite-strip, streamwise.

Figure 7.- Continued.

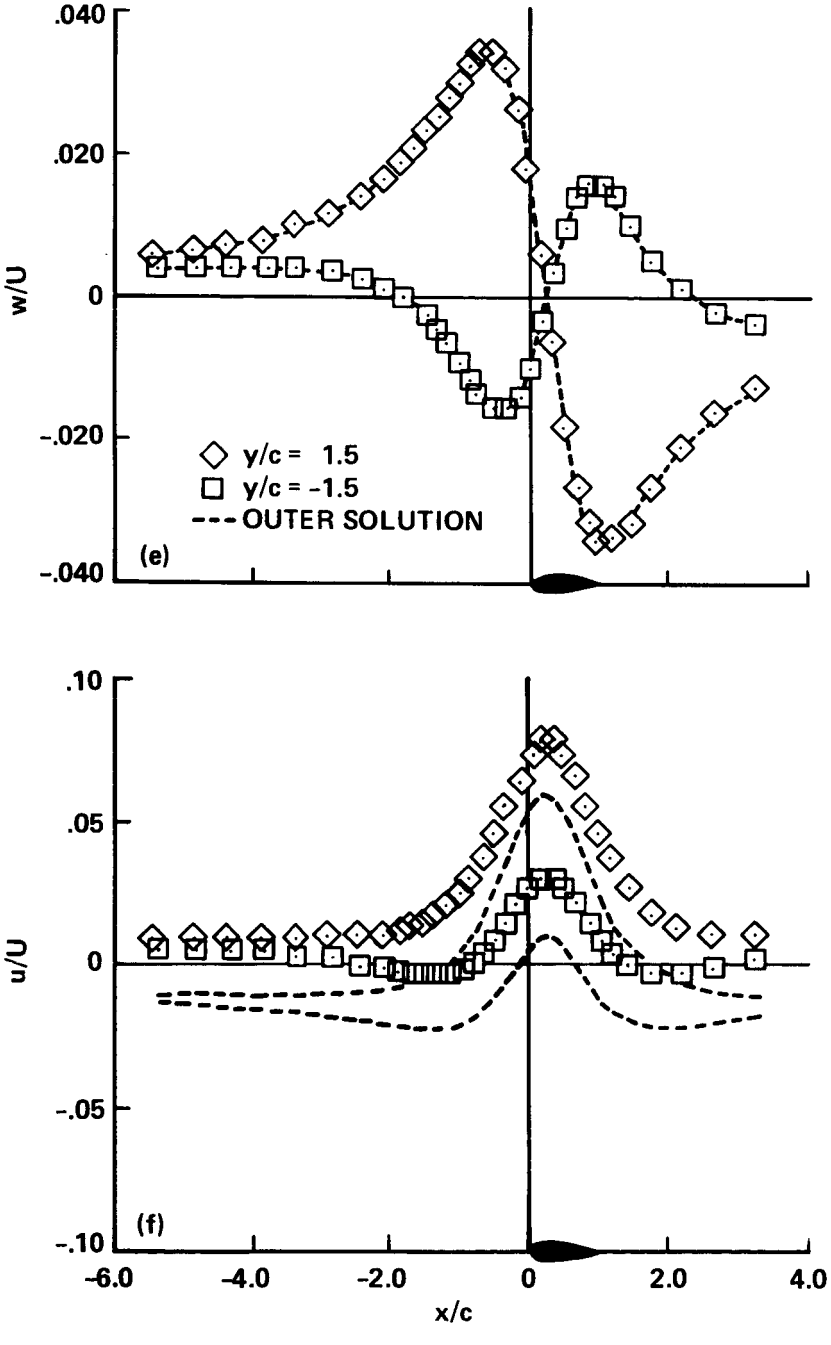

(e) Two-component/closed-contour, upwash.

(f) Two-component/closed-contour, streamwise.

Figure 7.- Concluded.

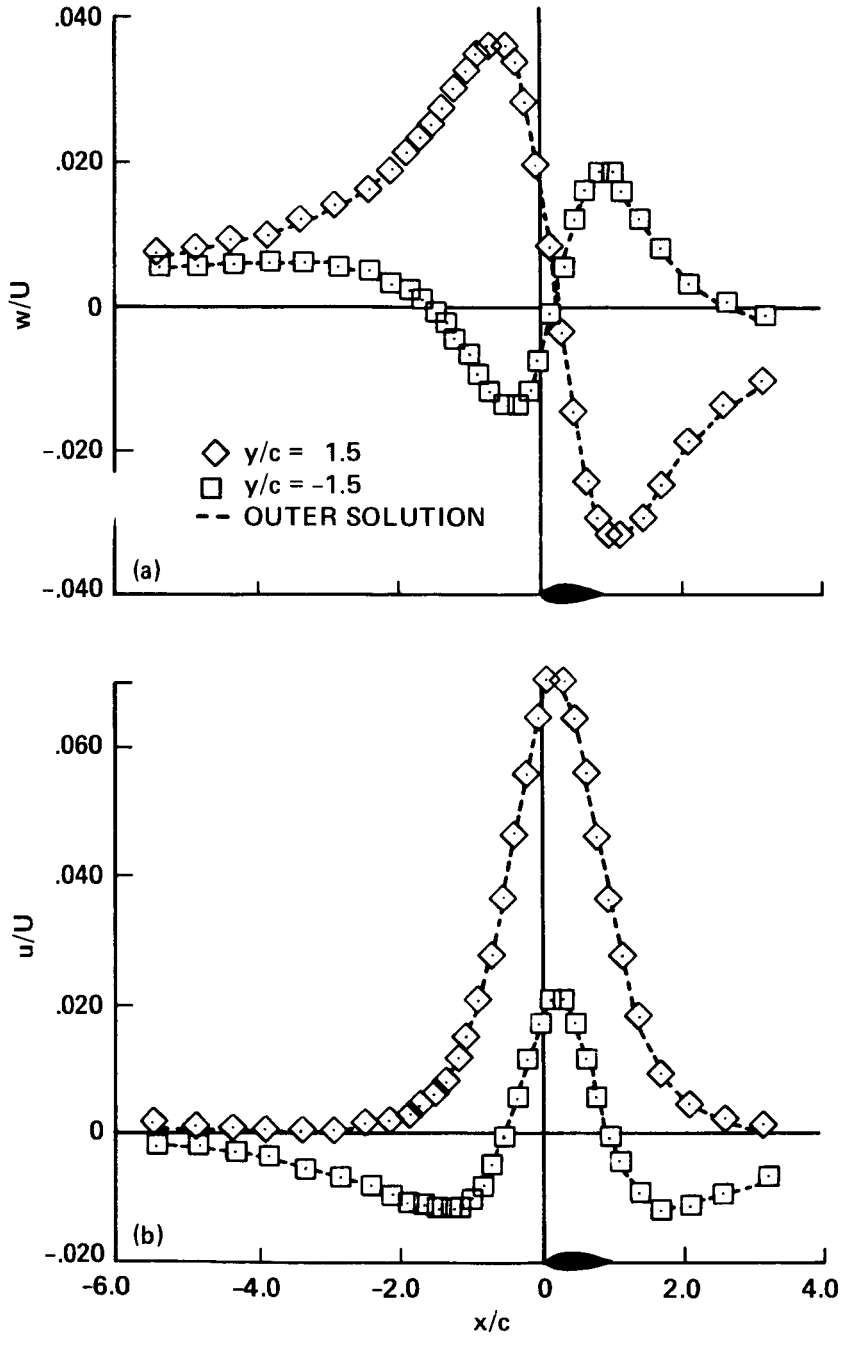

(a) One-component, upwash.

(b) One-component, streamwise.

Figure 8.- Effect of 0.1° flow-angle error on adaptive-wall solutions for a vortex and doublet in free air (M_∞ = 0.50, C_ℓ = 0.4, A = 0.4).

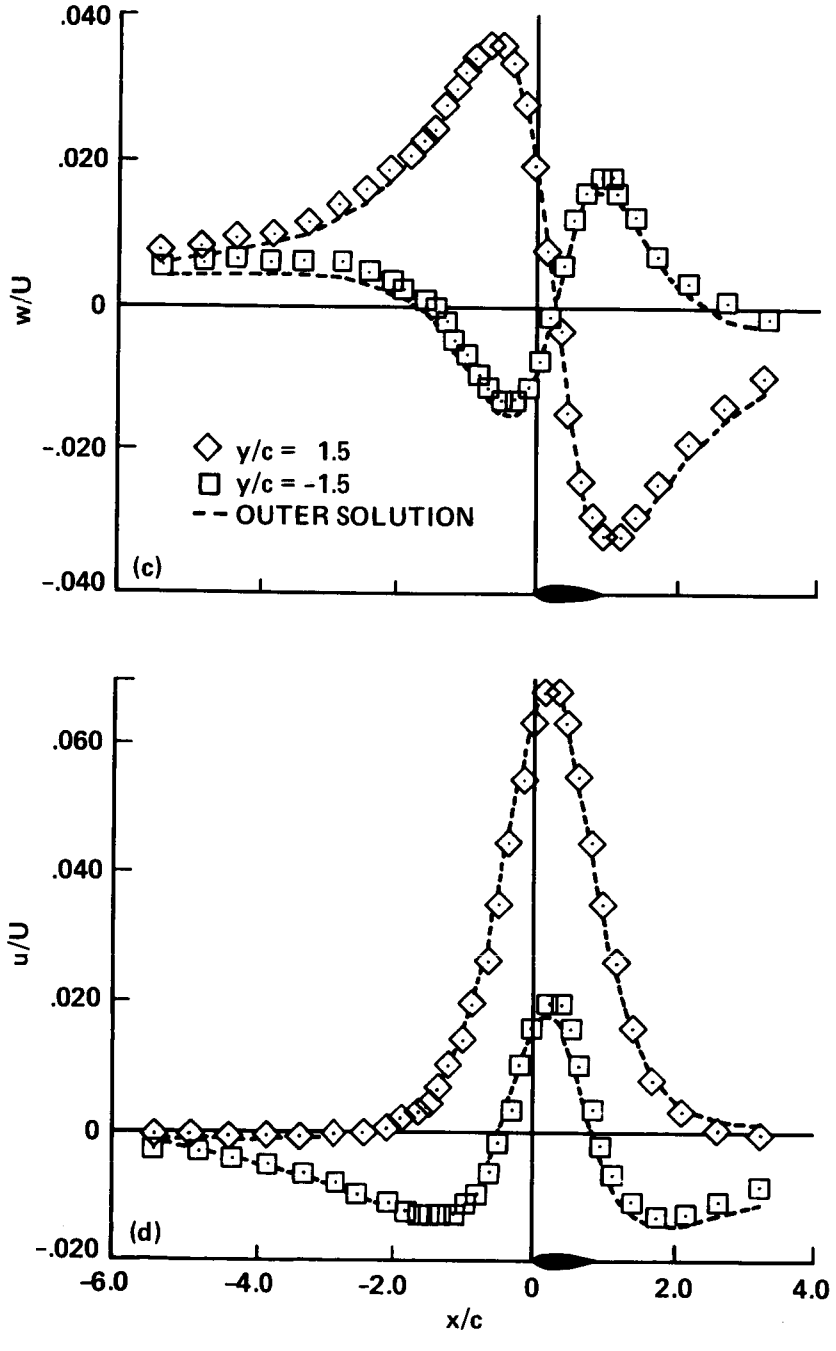

(c) Two-component/infinite-strip, upwash.

(d) Two-component/infinite-strip, streamwise.

Figure 8.- Continued.

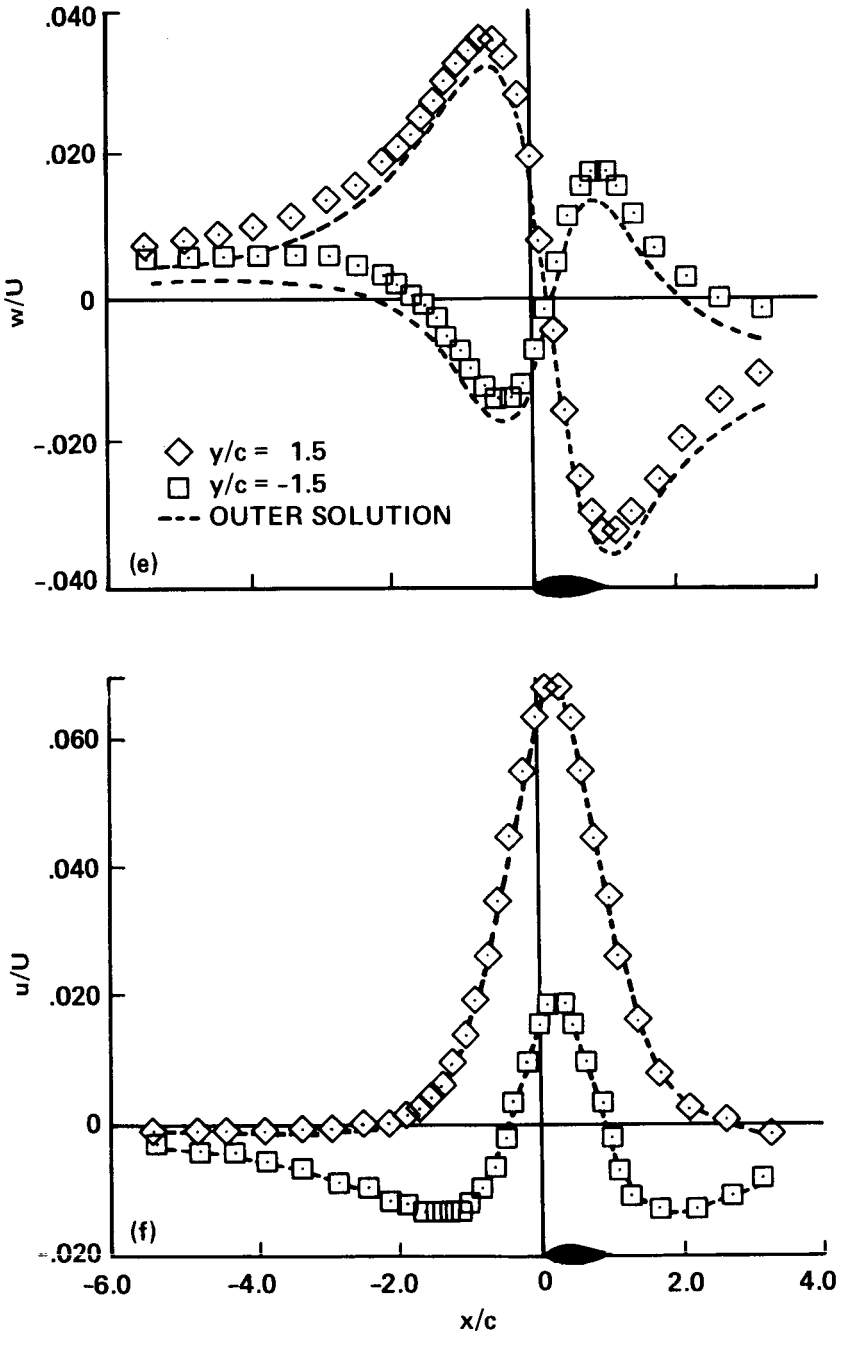

(e) Two-component/closed-contour, upwash.

(f) Two-component/closed-contour, streamwise.

Figure 8.- Concluded.

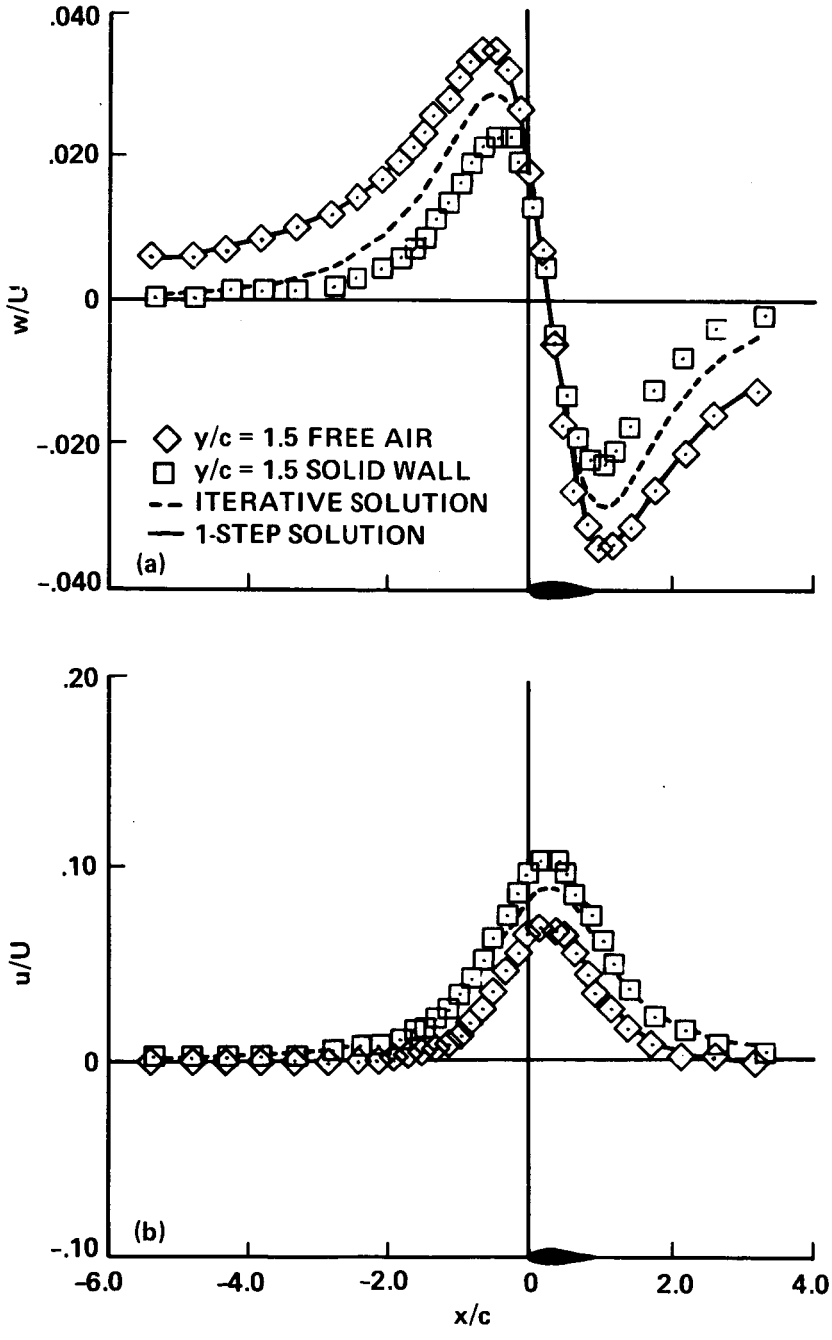

(a) One-component, upwash.

(b) One-component, streamwise.

Figure 9.- One-step adaptive-wall solutions for a vortex and doublet in a solid-wall wind tunnel (M_∞ = 0.50, C_ℓ = 0.4, A = 0.4).

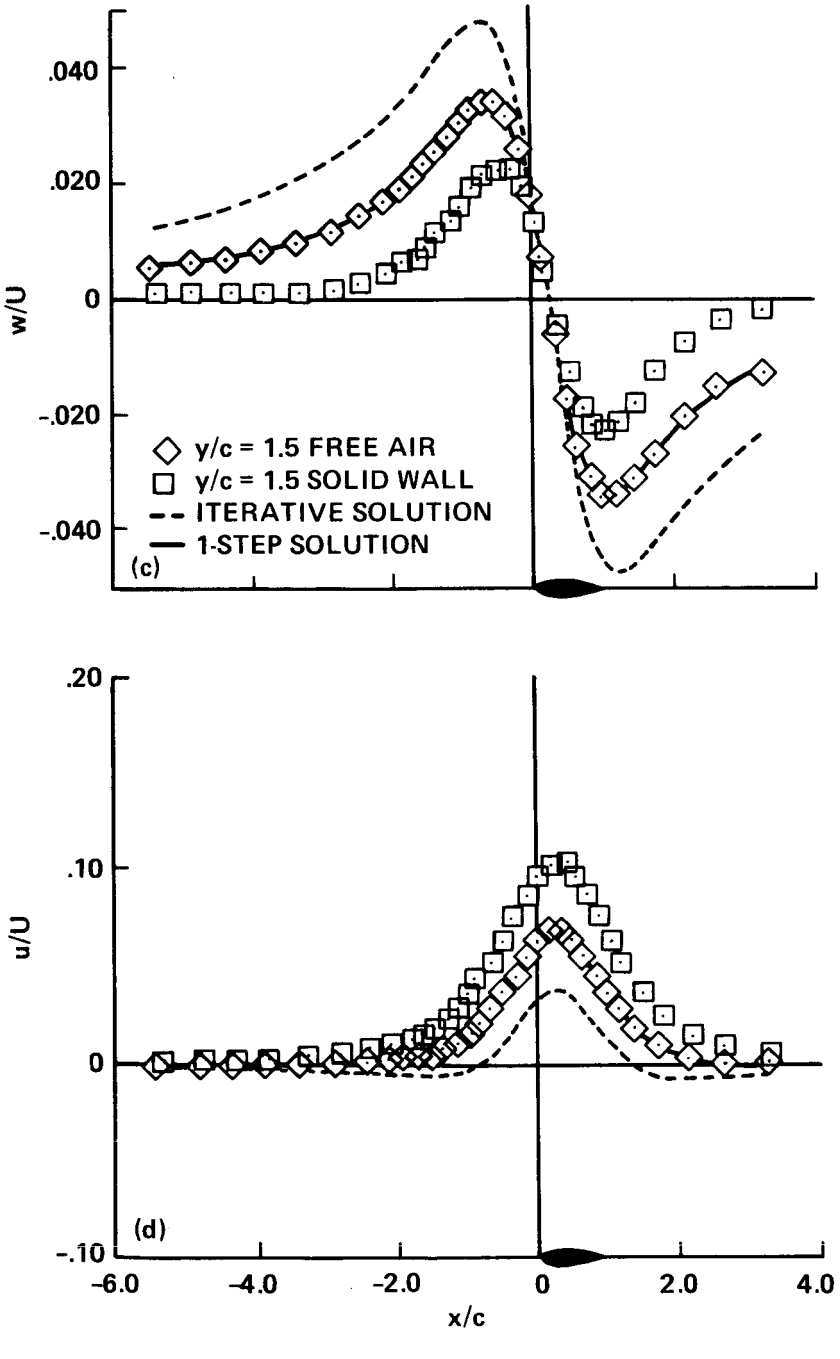

(c) Two-component/infinite-strip, upwash.

(d) Two-component/infinite-strip, streamwise.

Figure 9.- Continued.

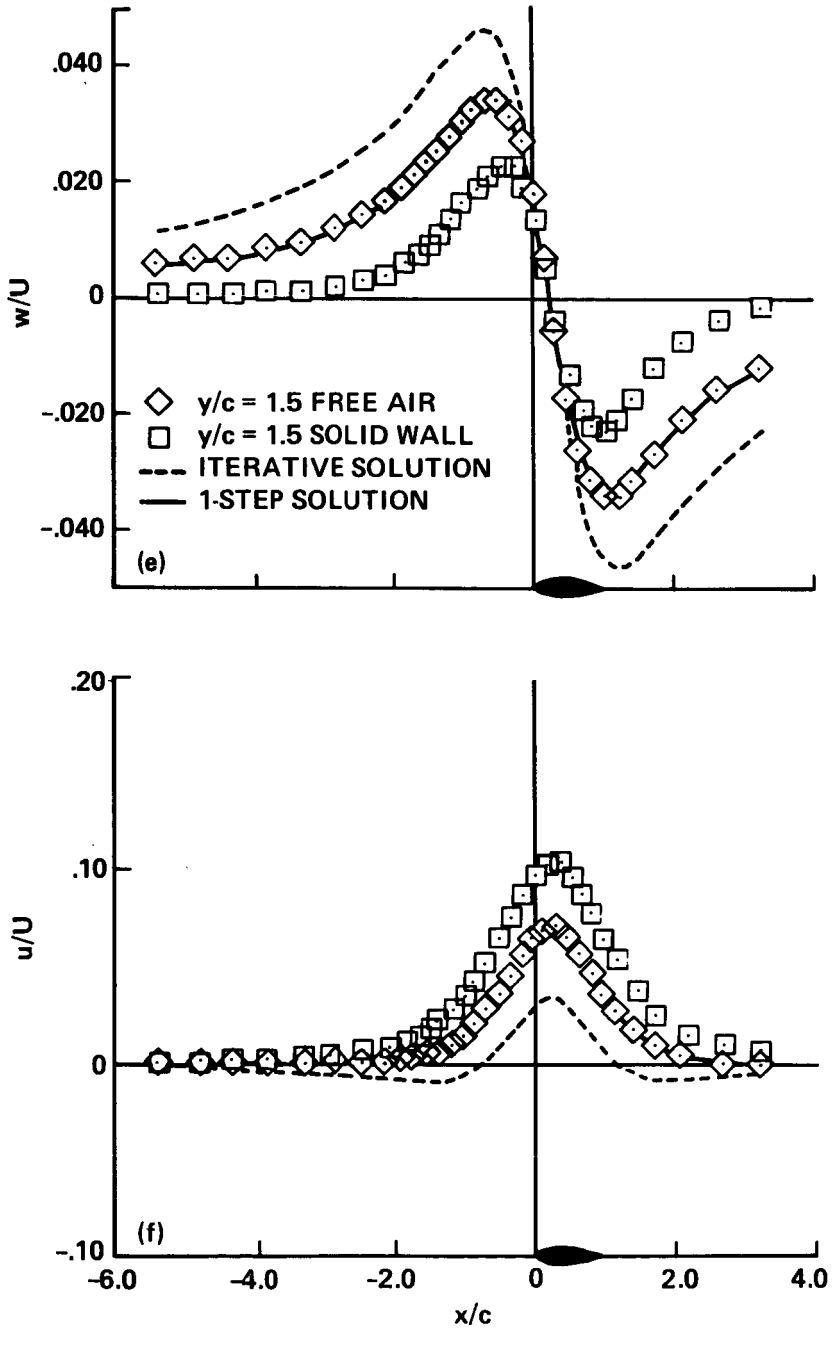

(e) Two-component/closed-contour, upwash.

(f) Two-component/closed-contour, streamwise.

Figure 9.- Concluded.

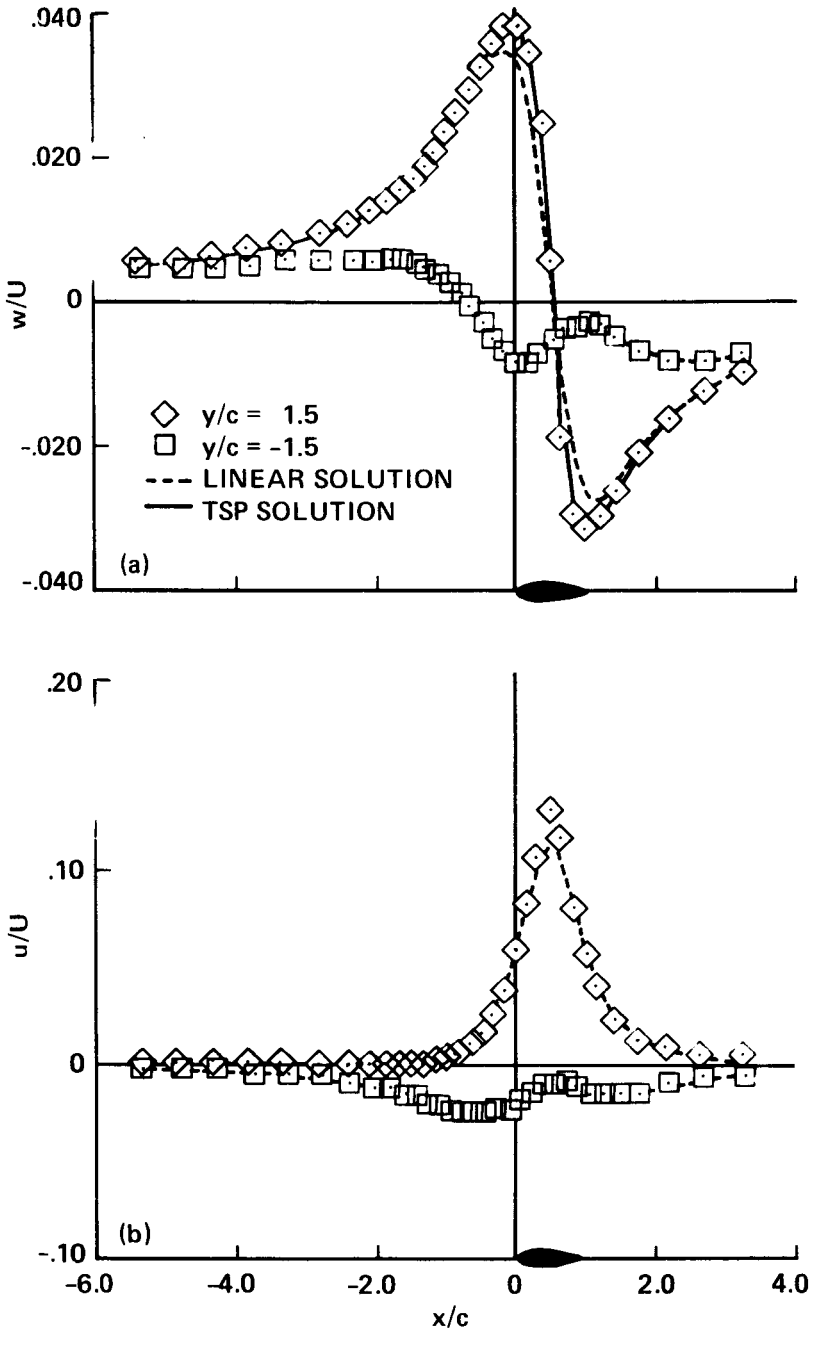

(a) One-component, upwash.

(b) One-component, streamwise.

Figure 10.- Adaptive-wall solutions for an NACA 0012 airfoil in free air (M_∞ = 0.80, α = 2.0°).

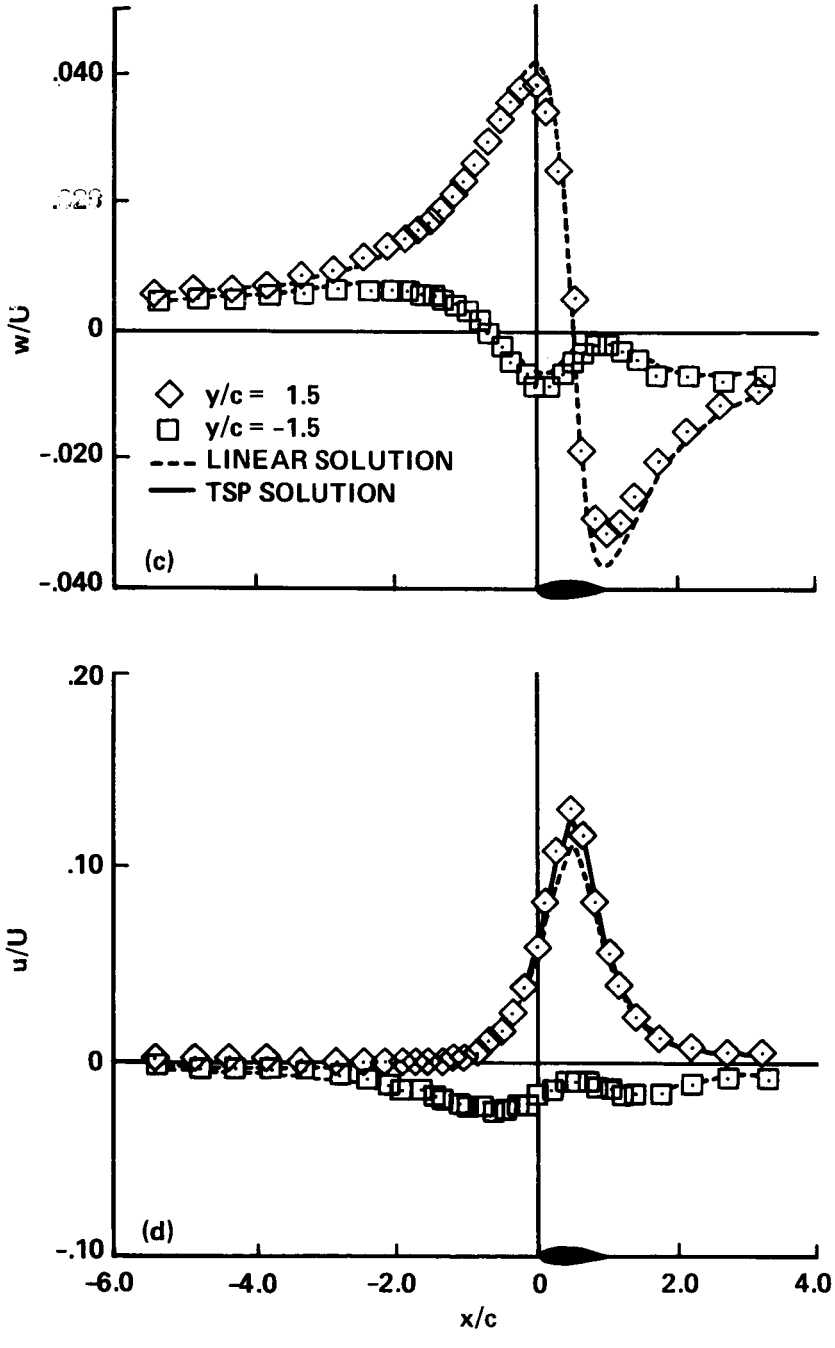

(c) Two-component/infinite-strip, upwash.

(d) Two-component/infinite-strip, streamwise.

Figure 10.- Continued.

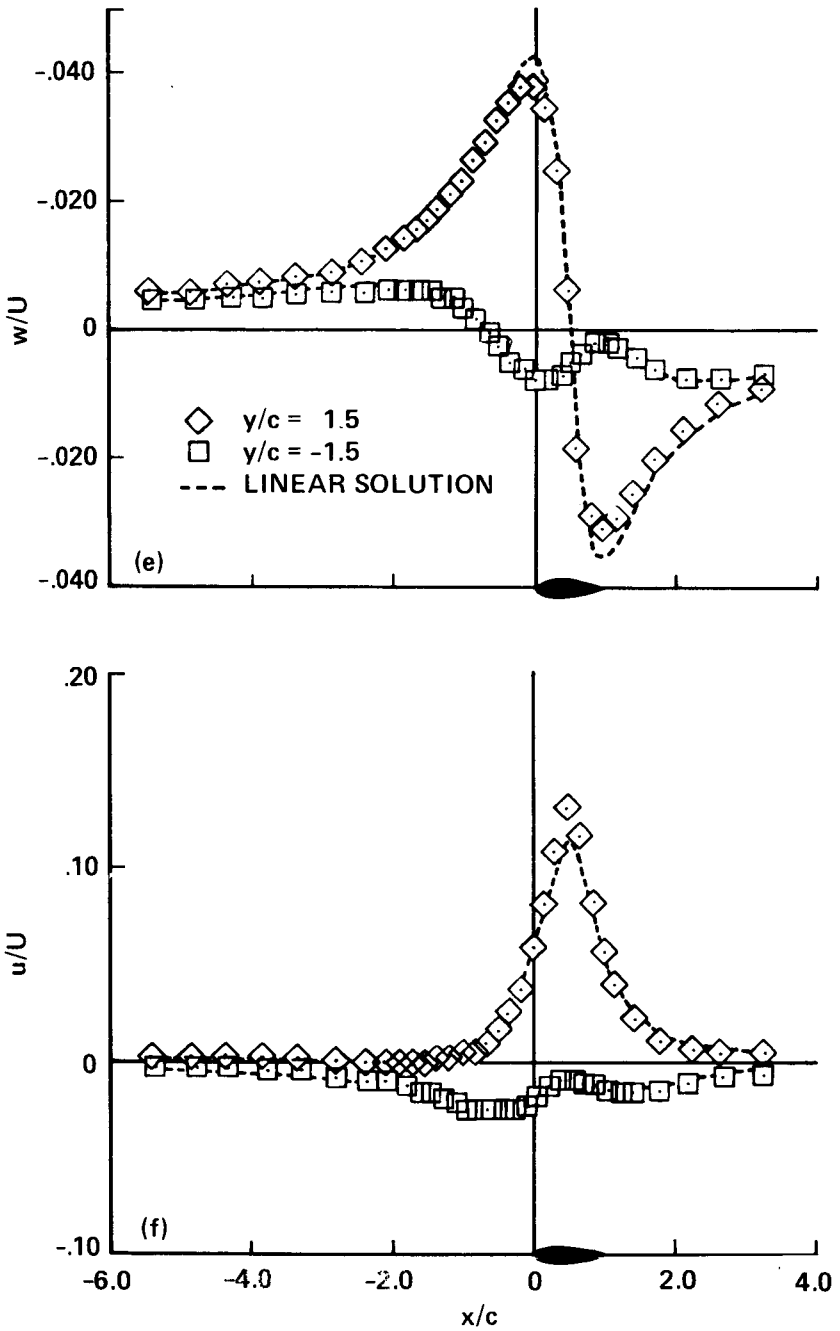

(e) Two-component/closed-contour, upwash.

(f) Two-component/closed-contour, streamwise.

Figure 10.- Concluded.

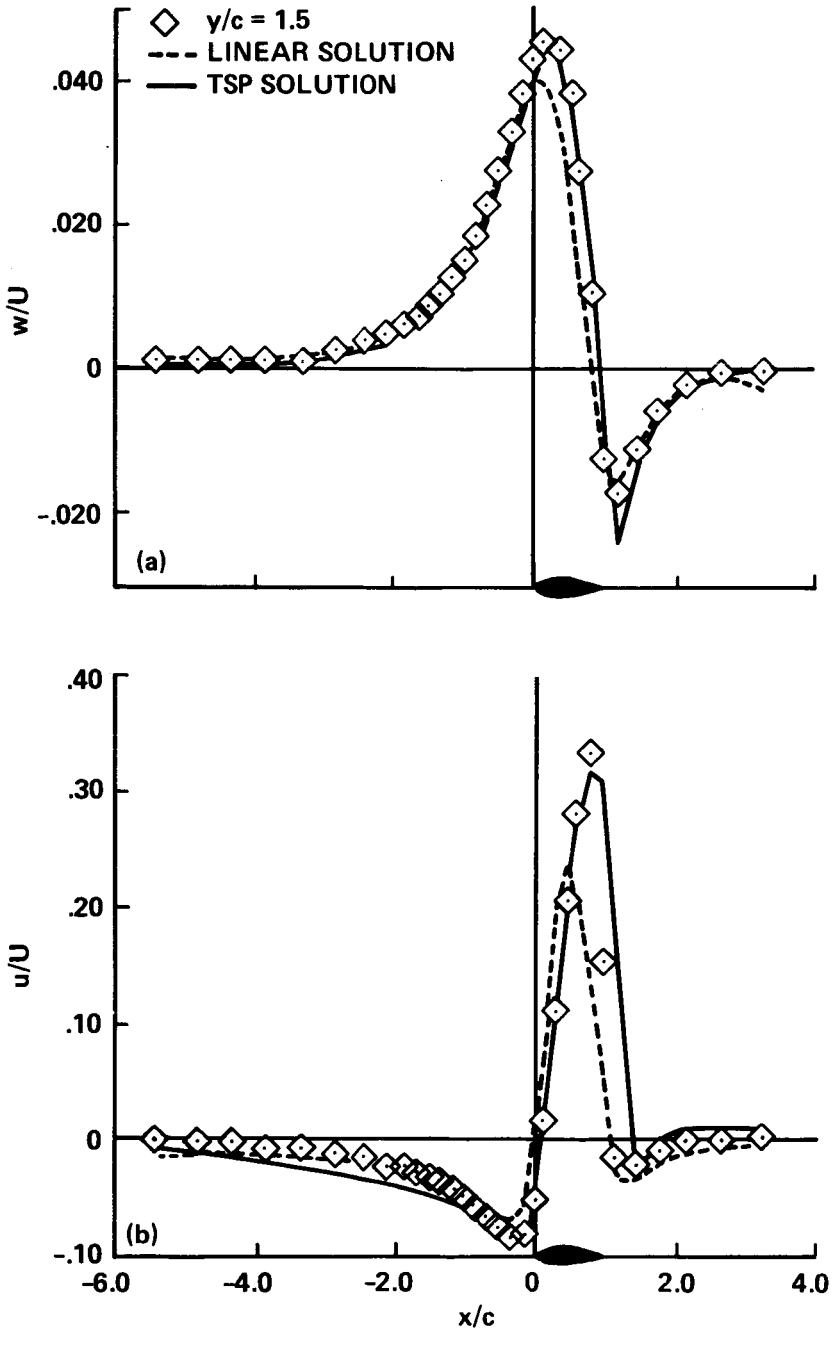

(a) One-component, upwash.

(b) Two-component, streamwise.

Figure 11.- Adaptive-wall solutions for an NACA 0012 airfoil in free air (M_∞ = 0.90, α = 0.0°).

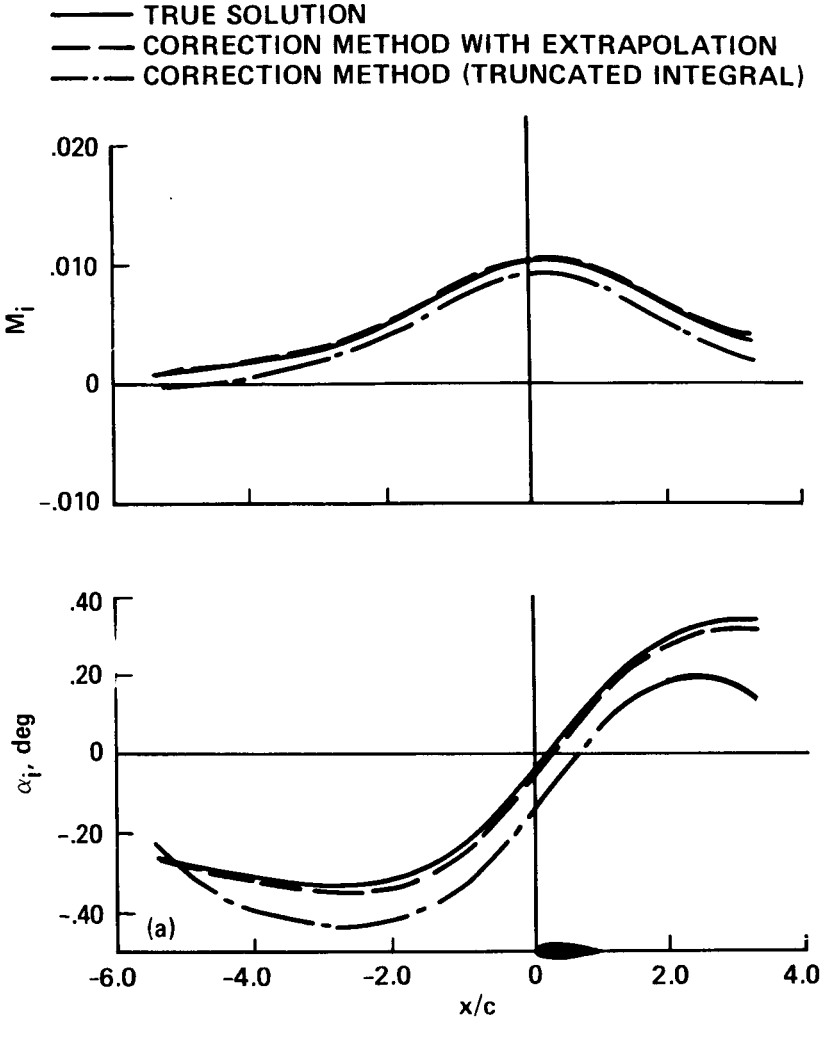

(a) One-component/two-contour/upwash.

Figure 12.- Wall-induced flow perturbations for a vortex and doublet in a solid-wall wind tunnel (M_∞ = 0.50, C_ℓ = 0.4, A = 0.4).

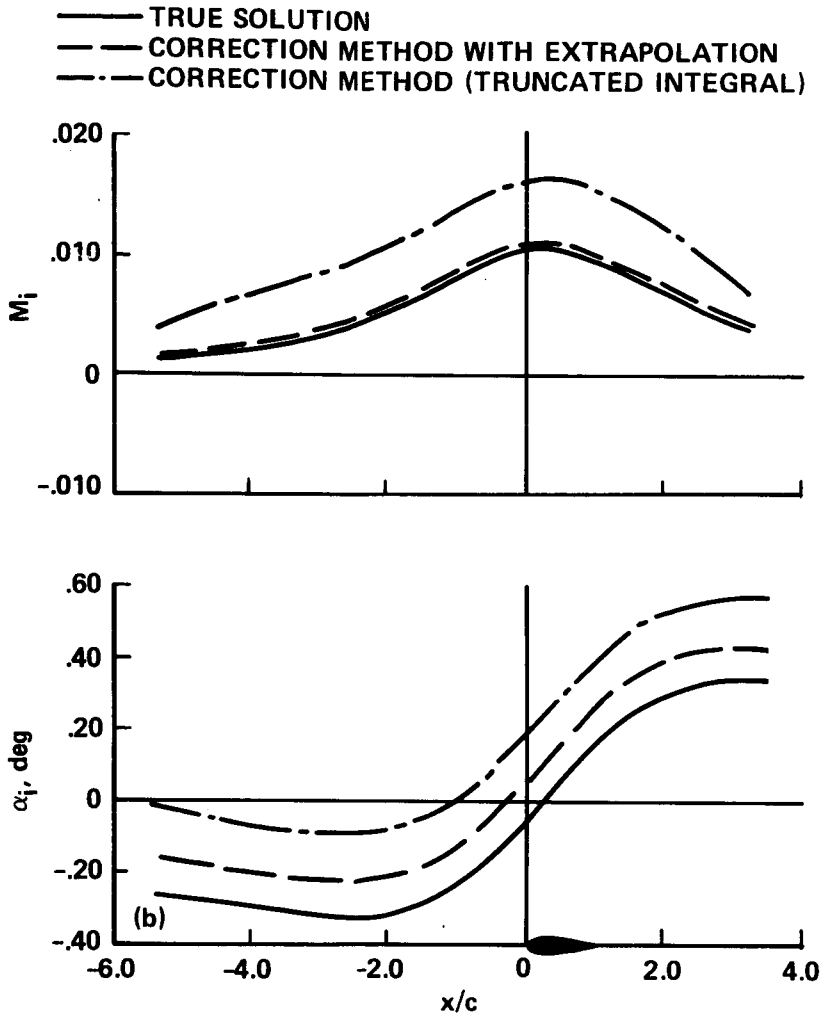

(b) One-component/two-contour/streamwise.

Figure 12.- Continued.

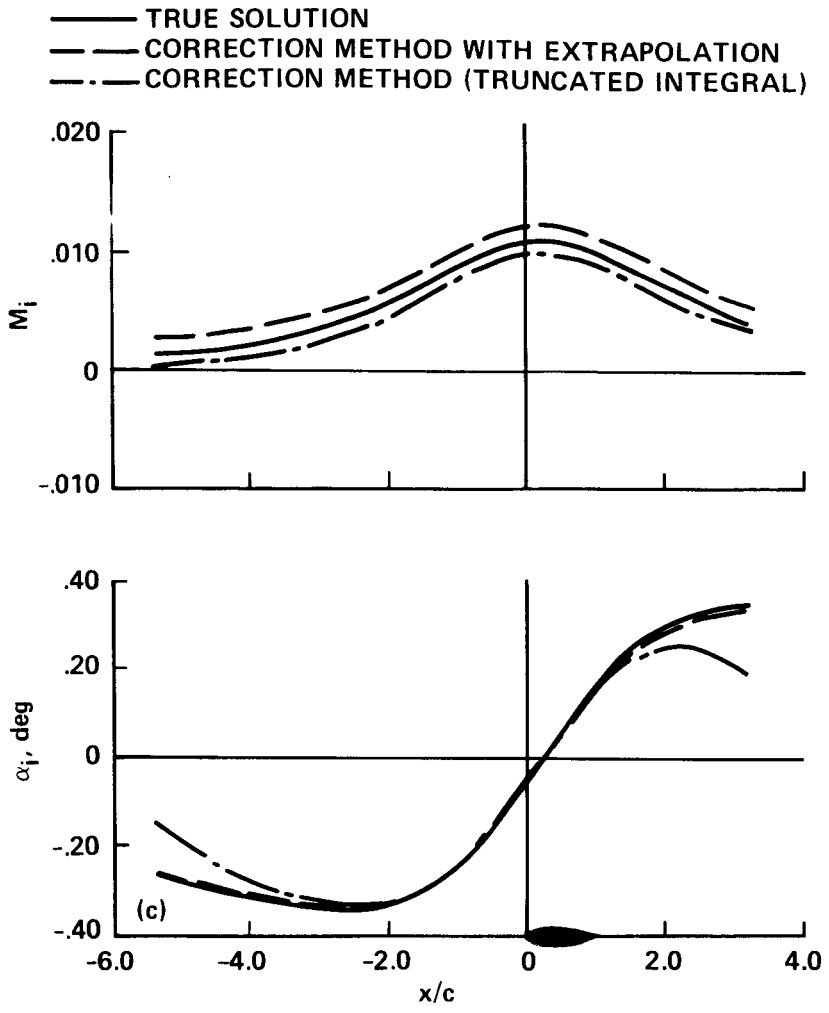

(c) One-component/one-contour/upwash.

Figure 12.- Continued.

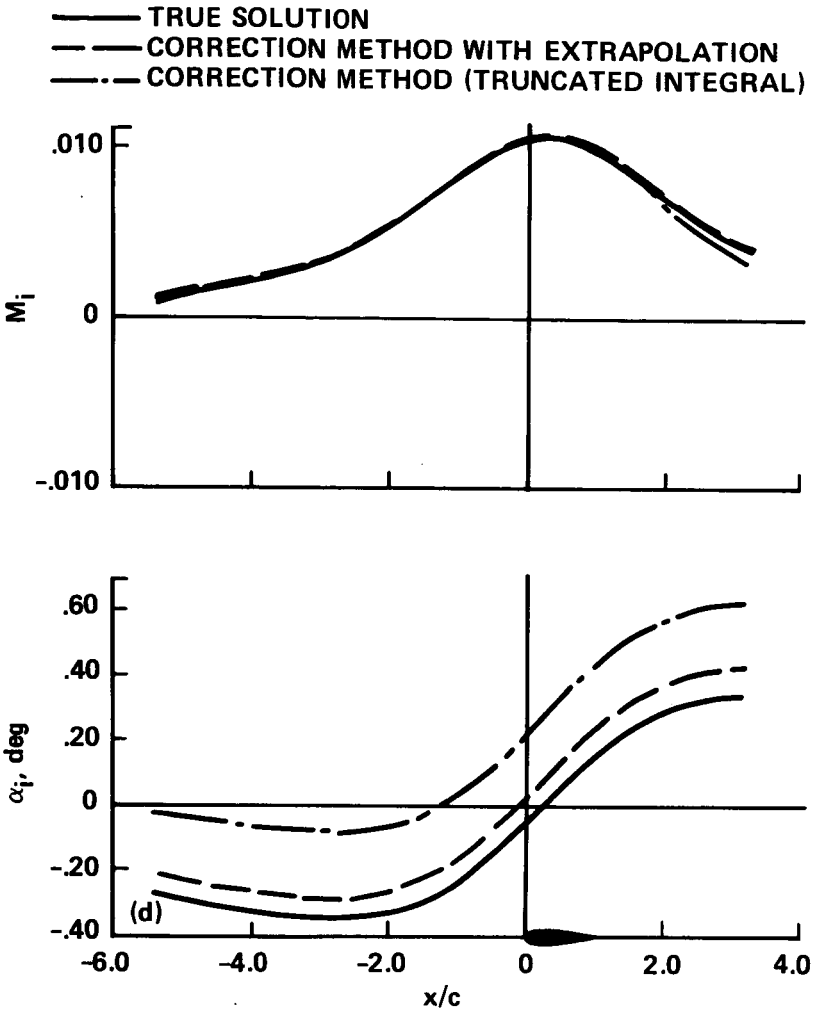

(d) One-component/one-contour/streamwise.

Figure 12.- Continued.

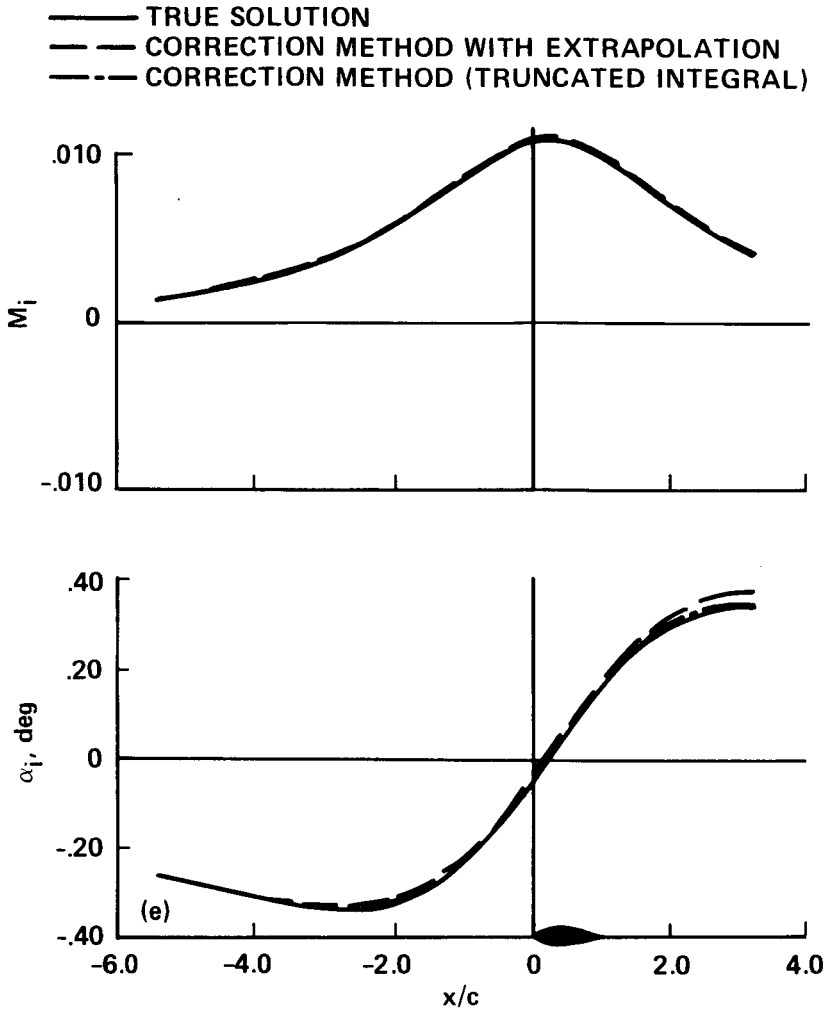

(e) Two-component.

Figure 12.- Concluded.

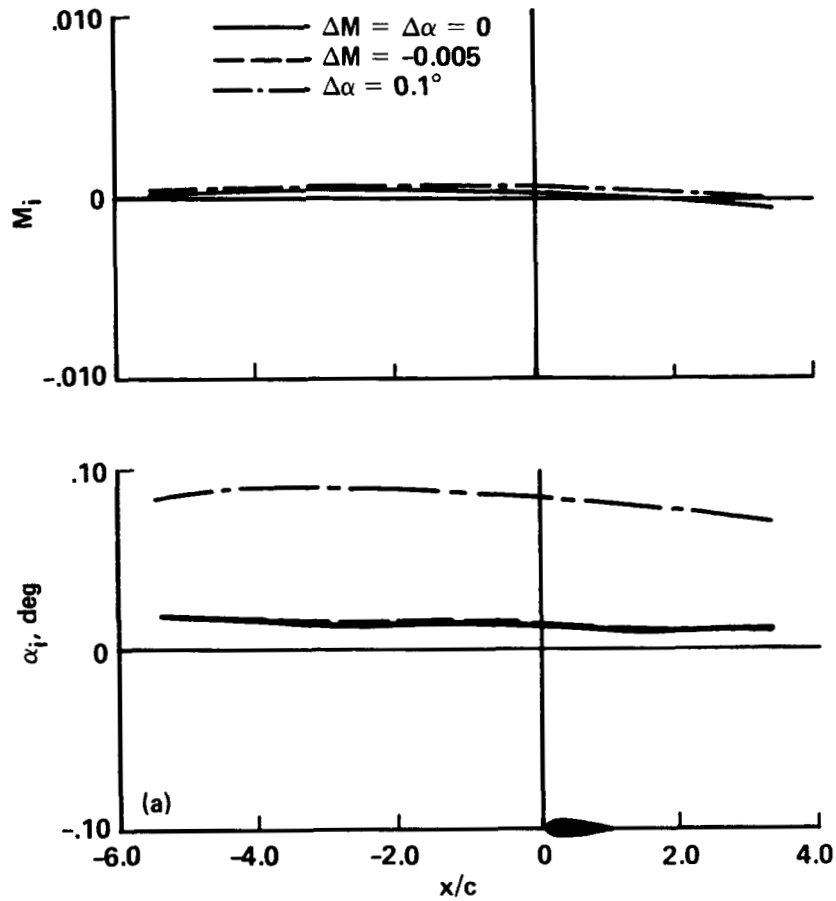

(a) One-component/two-contour/upwash.

Figure 13.- Wall-induced flow perturbations predicted for a vortex and doublet in free air, including the effects of Mach and flow angle errors (M_∞ = 0.50, C_ℓ = 0.4, A = 0.4).

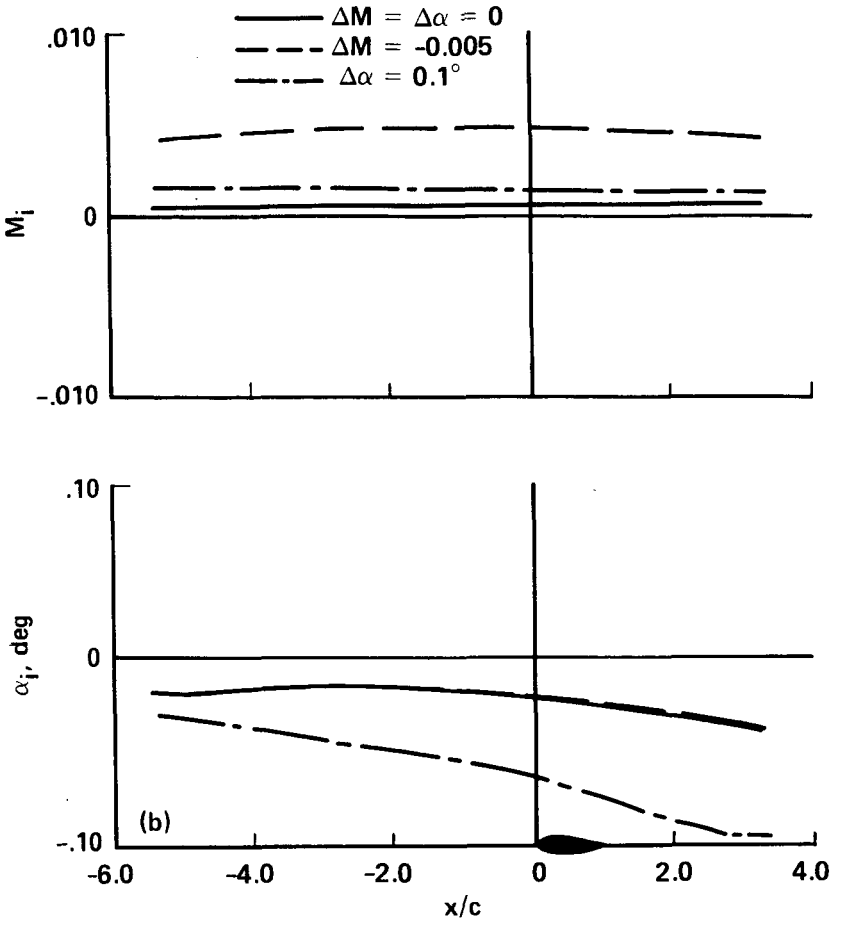

(b) One-component/two-contour/streamwise.

Figure 13.- Continued.

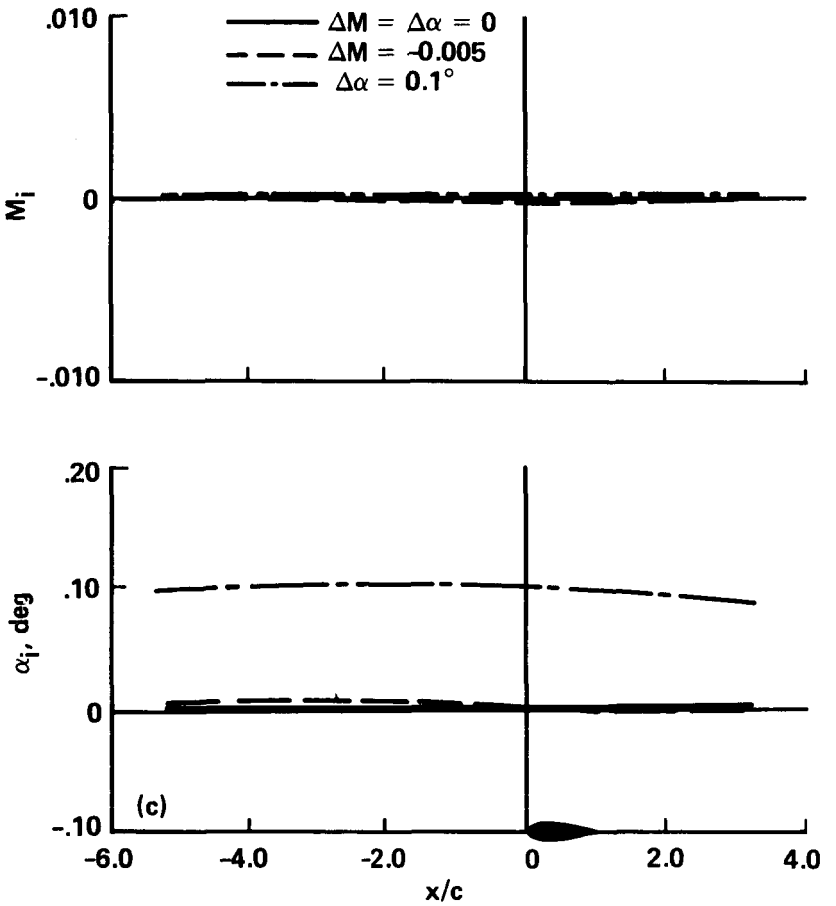

(c) One-component/one-contour/upwash.

Figure 13.- Continued.

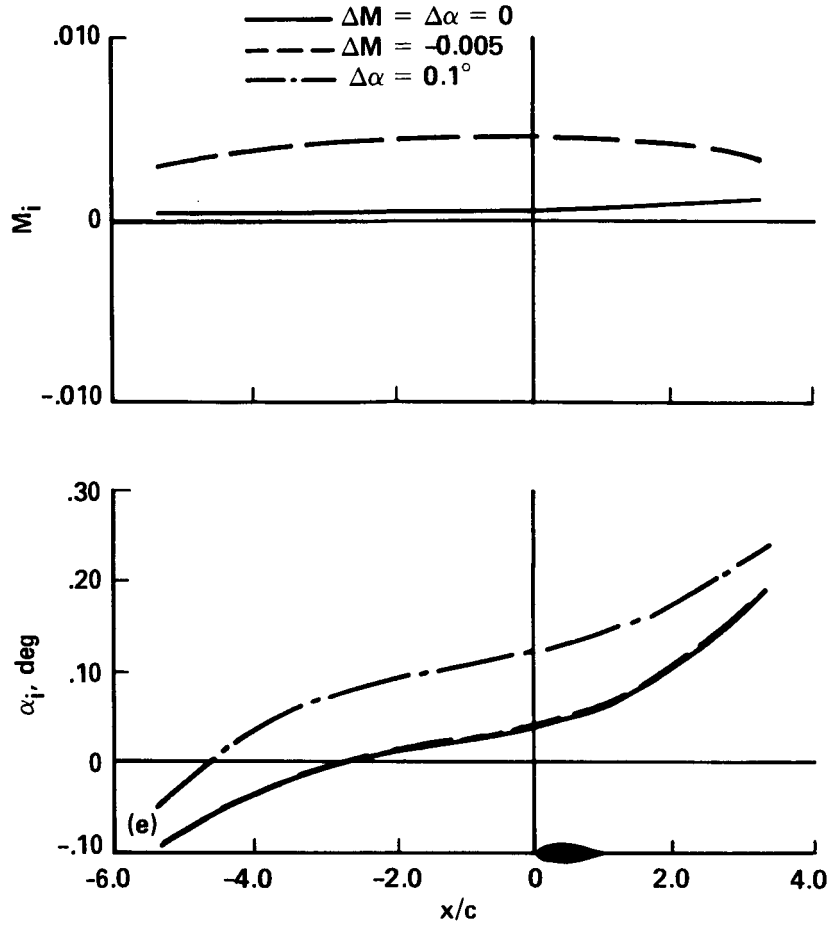

(e) Two-component/infinite-strip.

Figure 13.- Continued.

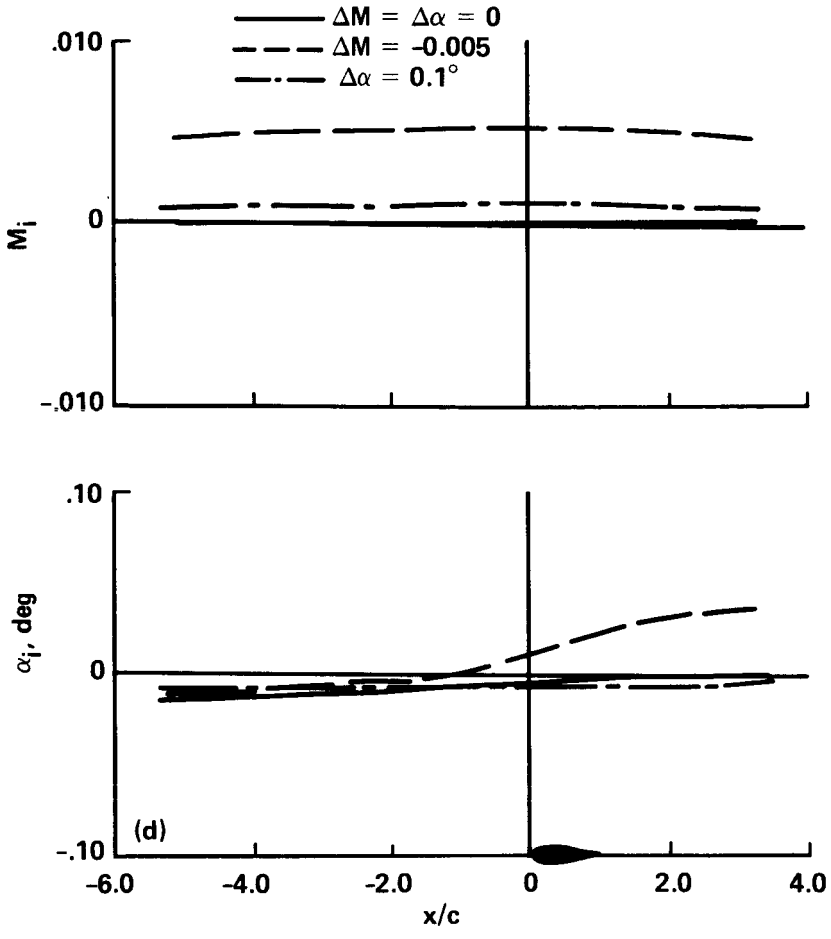

(d) One-component/one-contour/streamwise.

Figure 13.- Continued.

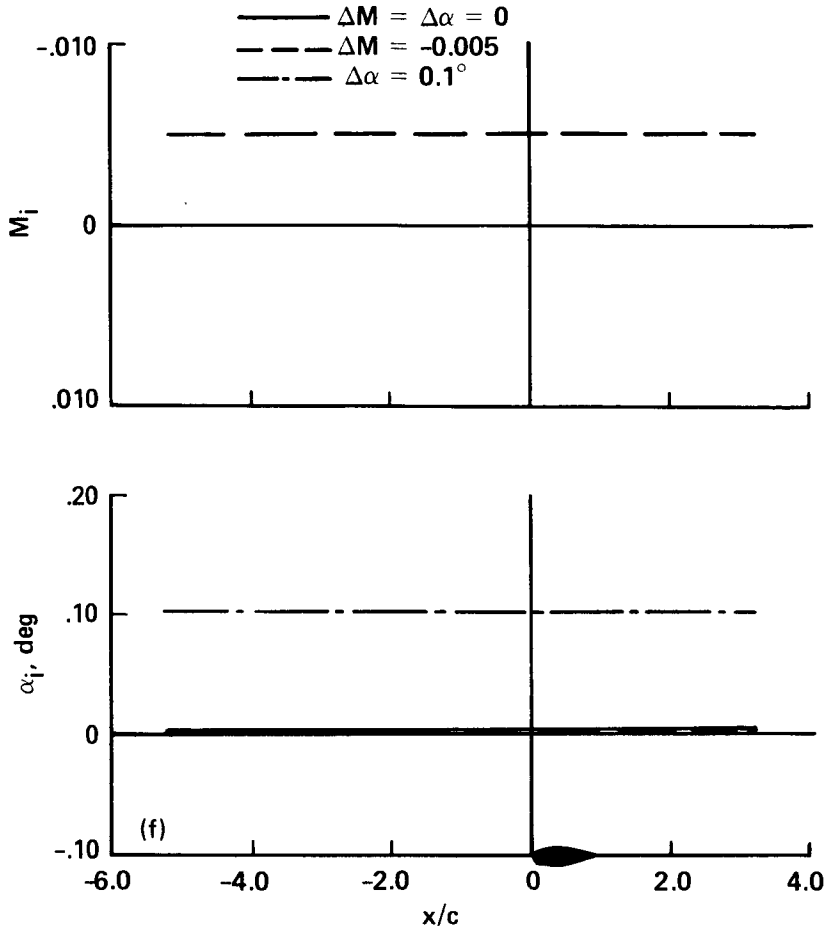

(f) Two-component/closed-contour.

Figure 13.- Concluded.

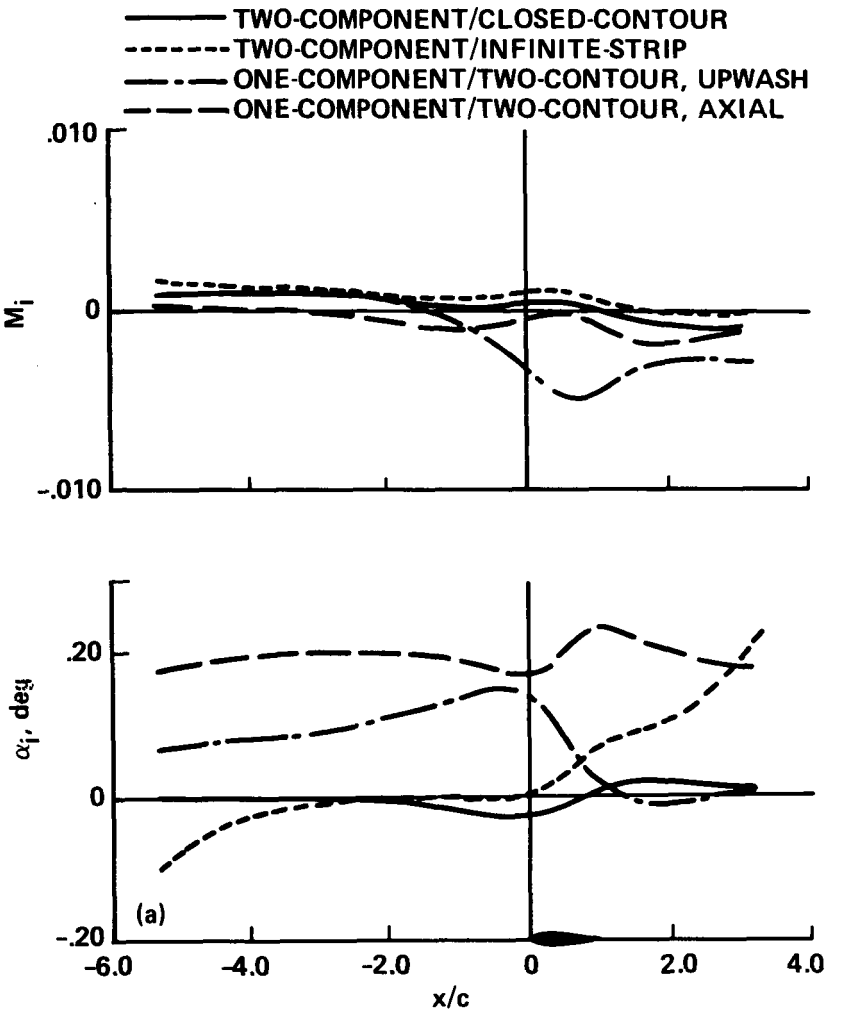

(a) Two-component and one-component/two-contour.

Figure 14.- Wall-induced flow perturbations predicted for an NACA 0012 airfoil in free air (M_∞ = 0.80, α = 2.0°).

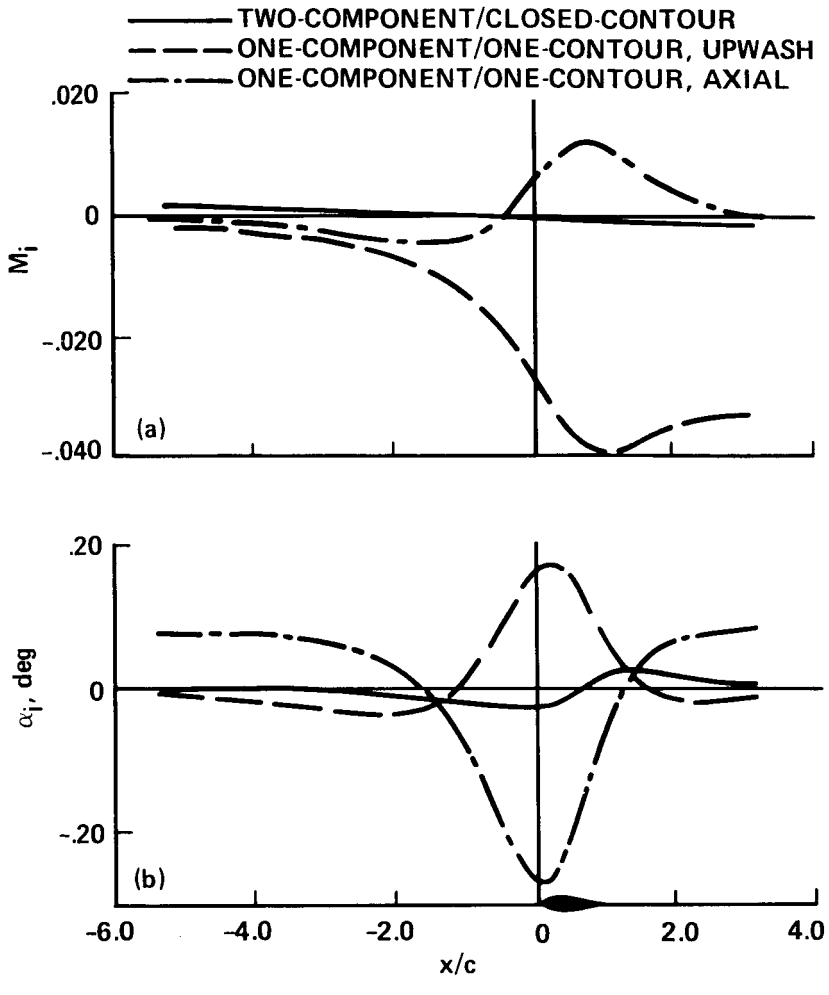

(b) Two-component/closed-contour and one-component/one-contour.

Figure 14.- Concluded.

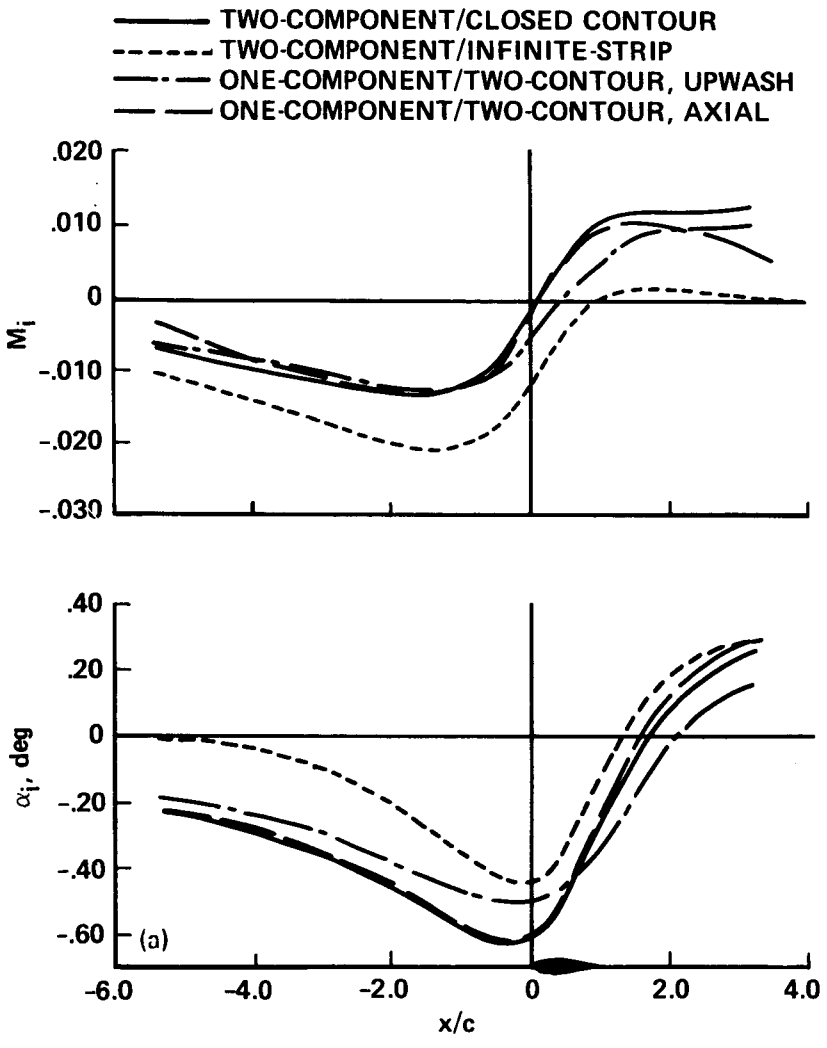

(a) Two-component and one-component/two-contour.

Figure 15.- Wall-induced flow perturbations predicted for an NACA 0012 airfoil in a porous-wall wind tunnel (M_∞ = 0.80, α = 2.0°, h/c = 4.0).

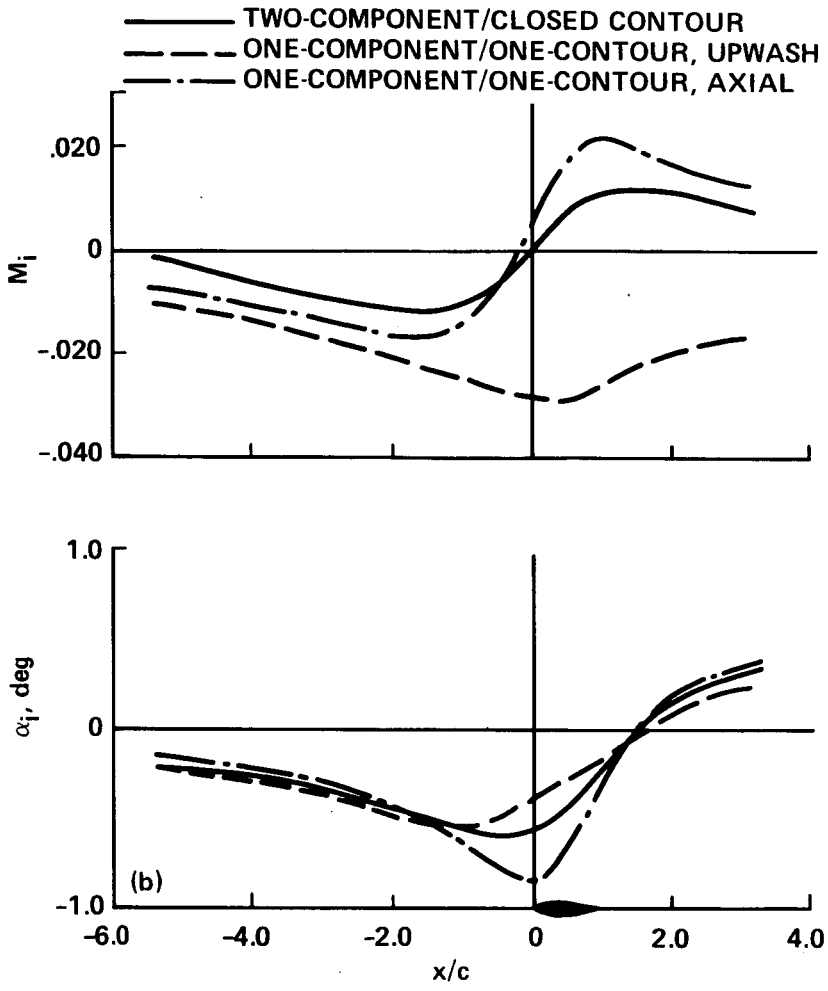

(b) Two-component/closed-contour and one-component/one-contour.

Figure 15.- Concluded.

1. Report No.	2. Government Accession No.	3. Recipient's Catalog No.
NASA TM-88252		

4. Title and Subtitle	5. Report Date
METHODS FOR ASSESSING WALL INTERFERENCE IN THE 2- BY 2-FOOT ADAPTIVE-WALL WIND TUNNEL	June 1986
	6. Performing Organization Code
7. Author(s)	8. Performing Organization Report No.
Edward T. Schairer	86249
	10. Work Unit No.
9. Performing Organization Name and Address	
Ames Research Center Moffett Field, CA 94035	11. Contract or Grant No.
	13. Type of Report and Period Covered
12. Sponsoring Agency Name and Address	Technical Memorandum
National Aeronautics and Space Administration Washington, DC 20546	14. Sponsoring Agency Code 505-65-01

15. Supplementary Notes

Point of Contact: Edward Schairer, Ames Research Center, MS 227-8, Moffett Field, CA 94035 (415)694-6288 or FTS 464-6288

16. Abstract

This paper discusses two types of methods for assessing two-dimensional wall interference in the adaptive-wall test section of the NASA Ames 2 × 2-Foot Transonic Wind Tunnel: (1) methods for predicting free-air conditions near the walls of the test section ("adaptive-wall" methods) and (2) methods for estimating wall-induced velocities near the model ("correction" methods). All of these methods are based on measurements of either one or two components of flow velocity near the walls of the test section. Each method is demonstrated using simulated wind tunnel data and is compared with other methods of the same type. The two-component adaptive-wall and correction methods were found to be preferable to the corresponding one-component methods because (1) they are more sensitive to, and give a more complete description of, wall interference; (2) they require measurements at fewer locations; (3) they can be used to establish free-stream conditions; and (4) they are independent of a description of the model and constants of integration.

17. Key Words (Suggested by Author(s))	18. Distribution Statement
Adaptive-wall Wall interface	Unlimited Subject category - 09

19. Security Classif. (of this report)	20. Security Classif. (of this page)	21. No. of Pages	22. Price*
Unclassified	Unclassified	59	A04

*For sale by the National Technical Information Service, Springfield, Virginia 22161